THERMOPHYSICAL PROPERTIES OF GLASS AND GLASS-CERAMIC COMPOSITES

by

LLOYD F. JOHNSON

Thesis submitted to the Faculty of the
Virginia Polytechnic Institute and State University
in partial fulfillment of the requirements for the degree of

MASTER OF SCIENCE

in

Materials Engineering

APPROVED:

D. P. H. Hasselman, Chairman

E. G. Henneke, II

J. R. Thomas, Jr.

July, 1987

Blacksburg, Virginia

THERMOPHYSICAL PROPERTIES OF GLASS AND GLASS-CERAMIC COMPOSITES

by

Lloyd F. Johnson

Committee Chairman: D. P. H. Hasselman
Materials Engineering

(ABSTRACT)

The thermal diffusivity and conductivity of several ceramic composites were determined experimentally to observe the effect of temperature, heat treatment and orientation on these properties.

The thermal conductivity and diffusivity of SiC whisker reinforced Ba-osumilite glass-ceramic exceeded that of SiC fiber reinforced osumilite due to higher thermal conductivity and diffusivity of the whiskers. An anisotropy was observed in thermal conductivity of the whisker composite due to whisker orientation normal to hot-pressing direc tion.

Thermal conductivity of carbon fiber reinforced borosilicate glass parallel to the fiber plane was about twice that of the normal orientation and of the matrix. Heating the composite to above 600^{o}C resulted in permanent decrease in thermal conductivity due to void formation by relaxation of the elastically bent fibers by viscous flow of the matrix.

Thermal conductivity of iniaxial carbon fiber reinforced lithia-aluminosilicate glass-ceramic was over ten times higher parallel to

the fibers than perpendicular. Permanent decrease of thermal conductivity normal to the fibers was due to matrix cracking caused by relief of internal stresses due to matrix crystallization and thermal gradients during fabrication.

Modification of the original theories of Maxwell and Rayleigh permitted derivation of expressions for thermal conductivity of composites of a continuous matrix with dilute concentrations of spherical and cylindrical geometries and of parallel flat plates with thermal resistance at the interfaces.

ACKNOWLEDGMENTS

The author thanks his committee chairman and advisor, Dr. D. P. H. Hasselman for support and the use of laboratory equipment. The other committee members, Dr. E. G. Henneke II and Dr. J. R. Thomas Jr., are thanked for their time and attention to this Thesis.

Dr. Larry D. Bentsen and Dr. R. Syed are recognized for sharing their time and knowledge of the laboratory equipment.

Financial support was provided by the Office of Naval Research, the Exxon Foundation and the Department of Materials Engineering.

TABLE OF CONTENTS

I. INTRODUCTION

Glasses and glass-ceramics are used with increasing frequency as the matrix for ceramic composite materials for service conditions involving high temperatures, severe thermal gradients and severe thermal stresses. Improvement of mechanical properties such as fracture toughness, tensile strength, creep resistance, impact resistance and hardness can be achieved as compared to single phase ceramics. Improved resistance to thermal shock can be attributed in part to increased thermal conductivity and thermal diffusivity of ceramic composites in which the reinforcing material has thermal conductivity and thermal diffusivity greater than the matrix phase. Design requirements may be that the thermal conductivity be as low as possible to conserve energy or to provide a thermal barrier which protects less refractory materials.

Thorough knowledge of the thermophysical properties of fiber or whisker reinforced ceramics is essential for engineering design of heat engines, heat shields or other components or structures operating at elevated temperatures or with severe thermal gradients.

Much research has been done on the characterization of thermophysical properties of homogeneous materials. Contemporary engineering applications require similar effort directed towards multiphase materials and anisotropic bodies. Characterization of such materials will permit tailoring of ceramic composites to meet demanding design cri-

teria while taking advantage of the most desirable properties of ceramics.

Glasses and glass-ceramics are often used as refractory structural materials due to their chemical properties and physical characteristics. It is the purpose of this Thesis study to examine the variables which affect the thermal diffusivity and thermal conductivity of fiber and whisker reinforced oxide glass and oxide glass-ceramic. The variables include temperature, heat treatment and orientation with respect to the fibers or whiskers.

The contents of this Thesis have been reported as publications in various journals [1-4].

II. EXPERIMENTAL PROCEDURE

A. General Description

Measurement of thermal conductivity and thermal diffusivity of solids has traditionally been by steady-state methods which are often time consuming and require large samples. Currently, a popular technique for measurment of thermal diffusivity is the flash method introduced by Parker et al [5]. The conditions required to obtain valid results include uniform absorption of an instantaneous pulse of energy on the front surface of a uniformly thick thermally insulated body at constant initial temperature. The sample thickness must be significantly less than the other dimensions in order to maintain one-dimensional heat flow in the center of the sample. A xenon flash lamp was the flash source in the early experiments, superseded by a pulsed laser in the experiments of Deem and Woods [6].

The preferred and most reproducible method to calculate thermal diffusivity by the flash method is to determine the time at which the temperature at the center of the back face of the sample reaches one half of the maximum temperature excursion. This is referred to as the half-rise time, designated $t_{1/2}$, and thermal diffusivity is calculated as:

$$a = A\ B\ L^2/t_{1/2} \qquad \text{(II-1)}$$

in which L is the sample thickness, and under the ideal conditions

described by Parker et al [5], A equals 0.1388 and B equals 1.

Consideration of experimental results under nonideal conditions has lead to determination of values for A and B for a variety of expermental conditions. The most difficult of the ideal requirements to obtain is the thermal insulation of the sample, especially at high temperature. This has been addressed by Cowan [7], Cape and Lehman [8], Clark and Taylor [9], Heckman [10] and Koski [11]. The analyses of Cowan, Clark and Taylor and Heckman, which are popularly used, are based upon measurement of the back surface temperature at times between five and ten half-rise times, and correction of the measured thermal diffusivity assuming a linear decrease of the back surface temperature during data acquisition. The effect of heat loss causes the value of A in Eq. II-1 to become less than 0.1388.

Another of the conditions which can be difficult to obtain is that the duration of the laser pulse is small compared to $t_{1/2}$. Low values of $t_{1/2}$ occur with thin samples of high thermal diffusivity. This effect has been examined by Cape and Lehman [8], Heckman [10] and Koski [11]. The pulse duration effect causes the value of B in Eq. II-1 to become greater than 1.

B. Apparatus and Method

The flash source which was a Nd-glass laser[1] generated a pulse

---

[1]Korad Industries, K-1

of 0.8 ms duration at a wavelength of 1.06 nm and variable energy per pulse of 30 to 55 J. A low energy He-Ne laser was mounted coaxially with the Nd-glass laser in order to align the optics of the entire system. A glass slide was used to deflect part of the laser pulse exiting the rear mirror into a silicon photodiode which initiated data acquisition concurrently with the firing of the laser.

For data acquisition at ambient temperature, the Nd-glass laser pulse was directed at the sample mounted on small metal pins about 1 cm in front of the active area of a liquid nitrogen cooled InSb photodetector.[1] The detector had a rise time of less than 0.1 microsecond and a wavelength response of 1.0 to 5.5 micron.

For data acquisition at elevated temperature the sample was placed in a graphite holder in the isothermal region of a water cooled graphite resistance furnace[2] with a nitrogen atmosphere at ambient pressure. The back face temperature of the sample was monitored by a Si photodiode[3]. The furnace temperature was manually controlled and monitored by a type K thermocouple up to 1000°C and at higher temperature by an optical pyrometer.[4]

The DC output from the detectors was connected directly to the

---

[1]Texas Instruments, Model ISV-381

[2]Astro Industries, Model 1000A

[3]EG&G Electro-Optics Div., Model SGD-100A

[4]Pyrometer Instrument Co., Micro Optical Pyrometer

input of a storage oscilloscope. The values of $t_{1/2}$ were measured directly from the oscilloscope screen. For determination of heat loss effects, the time and height of the temperature signal were recorded at the maximum transient temperature and at five to ten times $t_{1/2}$. The values of all time and temperature measurements, and the sample thickness determined by hand-held micrometer, were entered into an interactive computer program based upon the analyses of Heckman [10] and Koski [11], and run on an IBM PC microcomputer. Values of A, B and a were calculated by the computer program.

Accuracy of the apparatus and calculations were verified by measurement of a sample of grade AXM-5Q1 graphite and a sample of Armco iron.

Measurement of specific heat from 25°C to 600°C was made by differential scanning calorimetry[1] (DSC) with a dedicated microcomputer and software package provided by the manufacturer. Measurements were made in nitrogen atmosphere at ambient pressure. The DSC was calibrated using an indium melting point and heat of fusion standard provided by the manufacturer. Specific heat values were standardized using a single crystal of alpha-Al_2O_3.

Bulk density of samples was determined by the Archimedes method using mercury or deionized water as the fluid medium.

---

[1] Perkin-Elmer, Model DSC-4

Thermal conductivity of samples was calculated from:

$$K = a\ p\ C_p \qquad \text{(II-2)}$$

in which a is the thermal diffusivity, p is the bulk density and C_p is the specific heat at constant pressure.

III. SILICON CARBIDE - Ba-OSUMILITE GLASS-CERAMIC

A. Experimental

The matrix phase consisted of barium osumilite glass-ceramic with bulk composition approximately $BaO\ 2MgO\ 3Al_2O_3\ 9SiO_2$. Density at room temperature was 2.777 g cm^{-3}. The SiC whiskers obtained from a commercial source[1] had a mean diameter of 0.6 micron and length ranging from 10 - 80 microns.

Composites of the matrix phase and 30 w/o (26 v/o) whiskers with a density of 2.770 g cm^{-3} were the subject of an earlier study [13], which gave method of fabrication and mechanical property data.

The fiber reinforced composites, with a density of 2.680 g cm^{-3} consisted of the matrix reinforced with continuous SiC fibers[2] in 0^{o}-90^{o} cross-ply configuration. The composites were made by hot-pressing the stacked prepregs in the desired orientation in a graphite die at appropriate pressure and temperature with the fibers oriented normal to the hot-pressing direction. Crystallization of the matrix was achieved during the hot-pressing cycle. Following hot-pressing the fiber volume fraction was 35%. Figure 1 shows a photomicrograph of a polished section perpendicular to the fiber direction.

---

[1] ARCO Chemical Co., SC-9

[2] Nippon Carbon Co., NICALON

Figure 2 shows a scanning electron micrograph of a fracture surface of the whisker composite. By etching polished sections of the whisker composite in a dilute aqueous HF solution for sufficient time to remove most of the matrix, a preferred orientation of the whiskers was revealed. Scanning electron micrographs of etched polished sections parallel and perpendicular to the hot-pressing direction are shown in Figure 3.

Specimens for thermal diffusivity measurement were 10 x 8 x 2mm rectangular plates or 10 x 2mm circular plates cut from the hot-pressed billets with a diamond core drill and slow speed precision diamond saw. The specific heat specimens were 6 x 1mm circular plates.

Thermal conductivity was calculated using Eq. II-2. Changes in specimen dimensions during the measurement of thermal diffusivity were calculated using coefficients of thermal expansion $2.7 \times 10^{-6}\ ^{o}C^{-1}$ and $3.6 \times 10^{-6}\ ^{o}C^{-1}$ for the matrix and whisker composites, respectively, which were isotropic in thermal expansion. The corresponding data for the fiber reinforced composites were 3.1×10^{-6} and $3.3 \times 10^{-6}\ ^{o}C^{-1}$ parallel and perpendicular to the cross-ply fiber layers, respectively.

B. Results and Discussion

Figure 4 shows the experimental data for the thermal diffusivity of the matrix and whisker composites for directions of heat flow parallel and perpendicular to the hot-pressing direction. Figure 5

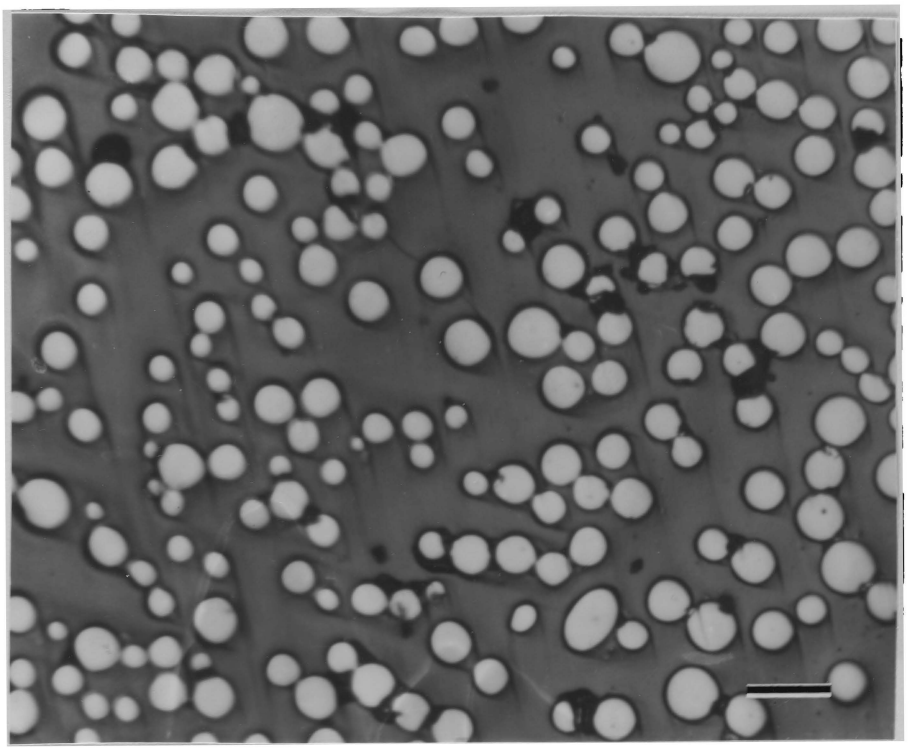

Figure 1. Optical micrograph of polished section of SiC fiber reinforced Ba-osumilite glass-ceramic (bar = 25 micron).

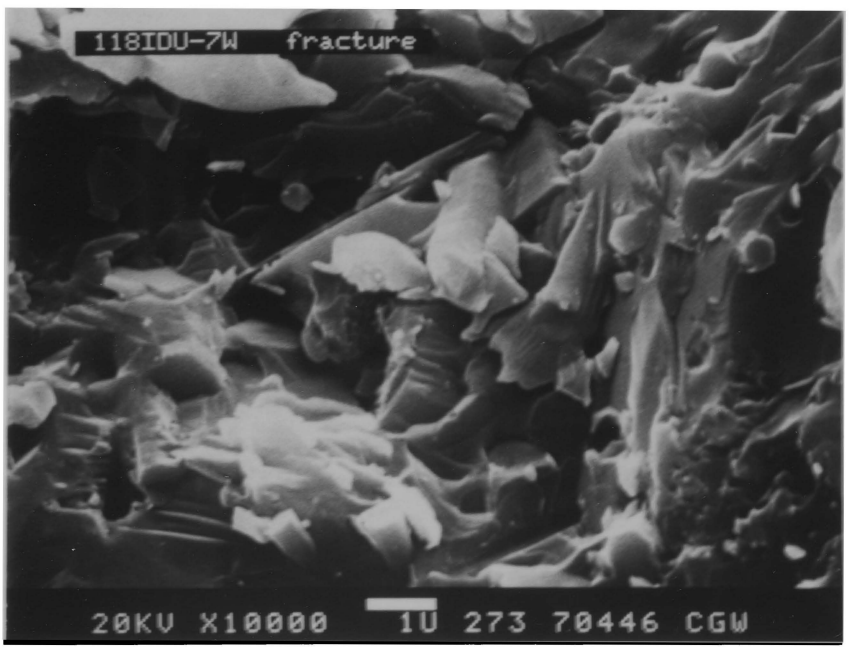

Figure 2. Scanning electron micrograph of fracture surface of SiC fiber reinforced Ba-osumilite glass-ceramic (bar = 1 micron).

a.

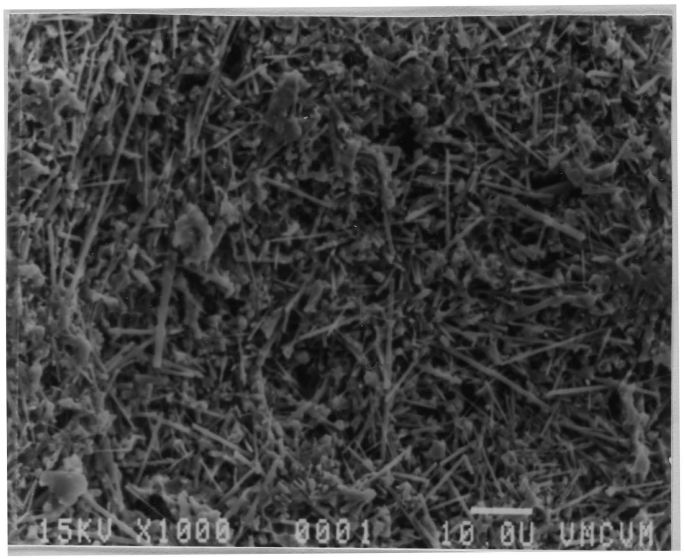

b.

Figure 3. Scanning electron micrographs of polished sections of SiC whisker reinforced Ba-osumilite glass-ceramic etched to remove most of the matrix, a: parallel and b: perpendicular to hot pressing direction (bars = 10 micron).

shows the data for the matrix and fiber reinforced samples for heat flow parallel to the plane of the fibers and perpendicular to the fiber plane. For both sets of composites the data obtained on cooling were identical within experimental error to those obtained on heating and were not included in the figures for purposes of clarity. The equivalence of data on heating and cooling implies that the materials of this study were not affected by irreversible effects such as matrix cracking or interfacial separation.

Comparison of the data in Figure 4 shows that the SiC whisker reinforcement results in an increase in thermal diffusivity by a factor of 4 at 25°C normal to the hot-pressing direction. The anisotropy in thermal diffusivity is attributable to preferred alignment of the whiskers perpendicular to the hot-pressing direction during densification. The anisotropy is in accordance with behaviour predicted by theory [14], that the thermal conductivity of composites is higher along a direction of preferred alignment of a second phase than in the transverse direction.

The thermal diffusivity of the whisker composites decreases with increasing temperature, exhibiting a negative temperature dependence. The thermal diffusivity of the matrix varies slightly with temperature as compared to the whisker composite. The thermal diffusivity of bulk crystalline SiC is high at 25°C, then decreases as temperature increases [15], thus causing the observed temperature dependence of the thermal diffusivity of the whisker composites.

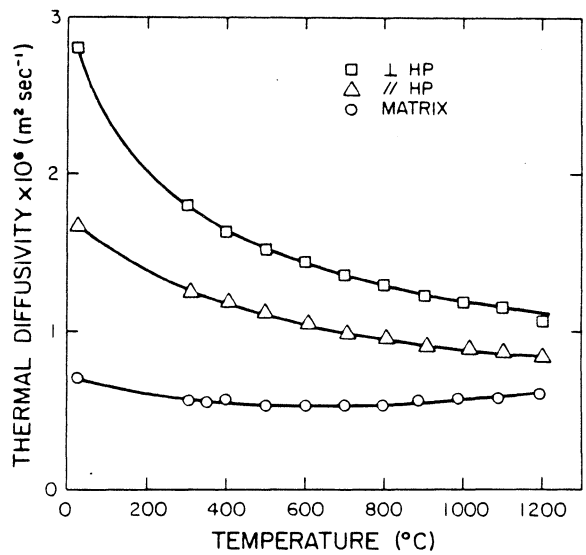

Figure 4. Effect of SiC whisker reinforcement on the thermal diffusivity of Ba-osumilite glass-ceramic.

The SiC fiber reinforced samples exhibit values of thermal diffusivity for both directions of heat flow about equal to corresponding values for the matrix phase. The positive temperature dependence of thermal diffusivity of the fiber composite is comparable to that of the matrix, and is indicative of a contribution of radiation to the transfer of heat.

The positive temperature dependence of the thermal diffusivity of the matrix and the fiber composites contrasts with the negative temperature dependence of that of the whisker composites. This is due to the high thermal diffusivity of the whisker composites at the lower temperatures. The SiC whiskers, which are single crystals, conduct heat by phonons more effectivly than the SiC fibers, and phonon transport is the primary mechanism of heat transfer at the lower temperatures. At the highest temperatures at which thermal diffusivity was measured, radiation contributes to the total heat transfer, to an extent observable in the data for the matrix and fiber composites but not in the data for the whisker composites, resulting in the temperature dependence of the data in Figs. 4 and 5.

Table 1 lists the data for the specific heat for the matrix phase without and with the SiC whisker and fiber reinforcement. The presence of the SiC causes a slight increase in specific heat of about 3% and 5% for the whisker and fiber reinforcement, respectively, at the higher temperatures.

Figures 6 and 7 show the values for the thermal conductivity for

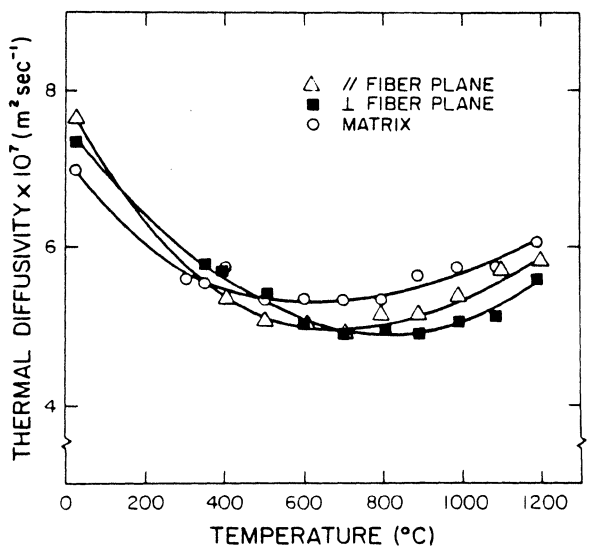

Figure 5. Effect of SiC fiber reinforcement on the thermal diffusivity of Ba-osumilite glass-ceramic.

Table 1. Specific heat ($J\ ^{o}K^{-1}g^{-1}$) of Ba-osumilite glass-ceramic matrix and composite with SiC whiskers or fibers.

Temperature (°C)	Ba-osumilite glass-ceramic	Composite with 27.3 vol % SiC whiskers	Composite with 35 vol % SiC fibers
25	0.694	0.693	0.698
100	0.786	0.816	0.810
200	0.868	0.914	0.914
300	0.932	0.974	0.984
400	0.988	1.020	1.058
500	1.027	1.058	1.089
595	1.051	1.084	1.104

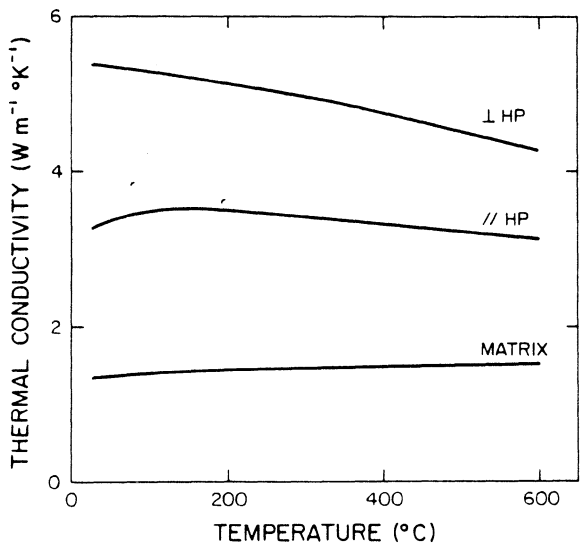

Figure 6. Effect of SiC whisker reinforcement on the thermal conductivity of Ba-osumilite glass-ceramic.

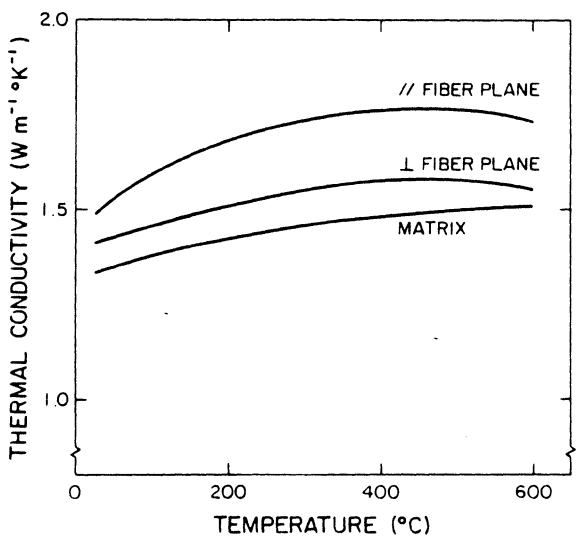

Figure 7. Effect of SiC fiber reinforcement on the thermal conductivity of Ba-osumilite glass-ceramic.

the matrix and SiC whisker and fiber composites, respectively, calculated with Eq. II-2, and the values for thermal diffusivity from the smooth curve drawn through the experimental data in Figures 4 and 5. The effect of the reinforcement on thermal conductivity is similar to the corresponding effect on thermal diffusivity. The temperature dependence of the thermal conductivity is due to the combined temperature dependence of the thermal diffusivity and specific heat. Because of the positive temperature dependence of the specific heat, the temperature dependence of the thermal conductivity is more positive than the temperature dependence of thermal diffusivity. If specific heat had been obtained above 600°C, the thermal conductivity of the specimens would have exhibited a positive temperature dependence, in particular the matrix and the fiber composites above 1000°C.

Comparison of Figures 6 and 7 shows that the thermal conductivity of Ba-osumilite composites can be adjusted by varying the reinforcing agent. If a composite was made from SiC fibers of the same type used in this study, chopped to the same aspect ratio as the SiC whiskers, then the chopped fiber composite would have about the same fracture toughness and fracture strength as the whisker composite. The thermal diffusivity and thermal conductivity of the whisker composite would be significantly greater, and hence the thermal shock resistance of the whisker composite would be greater.

This allows tailoring of the thermophysical properties of the Ba-osumilite composites while keeping desirable mechanical properties.

IV. CARBON FIBER - BOROSILICATE GLASS

A. Experimental

The matrix phase consists of borosilicate glass with density 2.23 g cm^{-3} and composition identical to Pyrex^{R} glass. Its thermal expansion coefficient is 3.6 x 10^{-6} $^{o}C^{-1}$.

The carbon fibers are Celion 6000[1], the latter number indicating the number of fibers per tow. Young's modulus of the fibers is about 235 GPa. The mean fiber diameter is about 7 microns.

The fibers were received as discontinuous fiber mats with a mean fiber length of 1.9 cm. Plies of carbon fiber mats were cut to size, impregnated with a slurry containing the glass powder, dried and stacked in a carbon tool and consolidated by hot-pressing at appropriate temperatures and pressures. The resultant composites as panels 10.2 x 10.2 x 2.0 cm had a random distribution of the carbon fibers perpendicular to the hot-pressing direction. The thermal expansion coefficient in the plane of the fibers is 1.7 x 10^{-6} $^{o}C^{-1}$, the corresponding value perpendicular to the plane of the fibers is 4.3 x 10^{-6} $^{o}C^{-1}$. The mechanical behavior of these composites was reported previously [16].

Figure 8 shows an optical micrograph of a polished section perpendicular to the plane of the fibers. The circular or near circular crossection of the fibers indicates the preferred orientation of the fibers within the hot-pressed panel.

Figures 9a and 9b show scanning electron micrographs of fracture

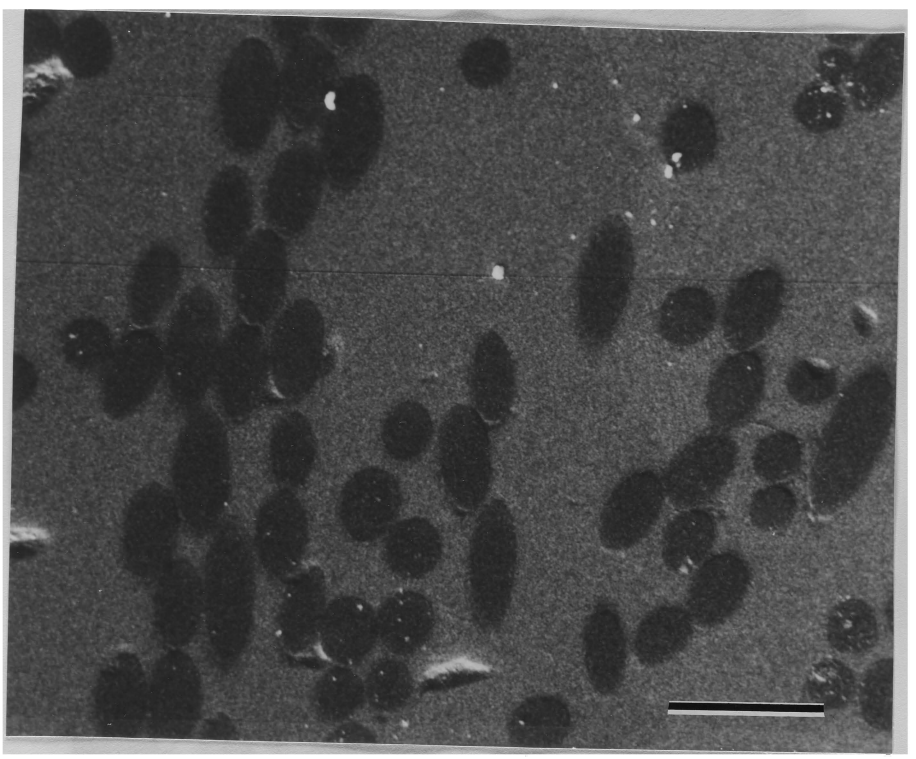

Figure 8. Optical micrograph of polished section of carbon fiber reinforced borosilicate glass (bar = 20 micron).

a.

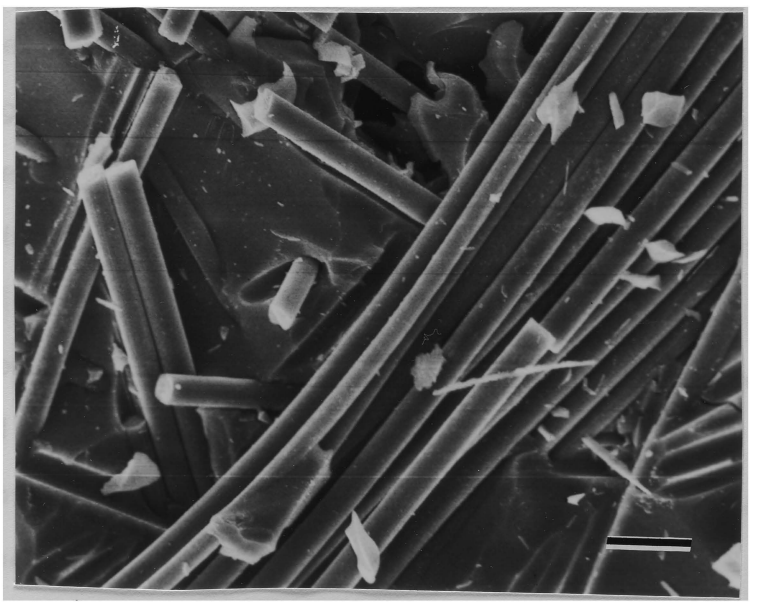

b.

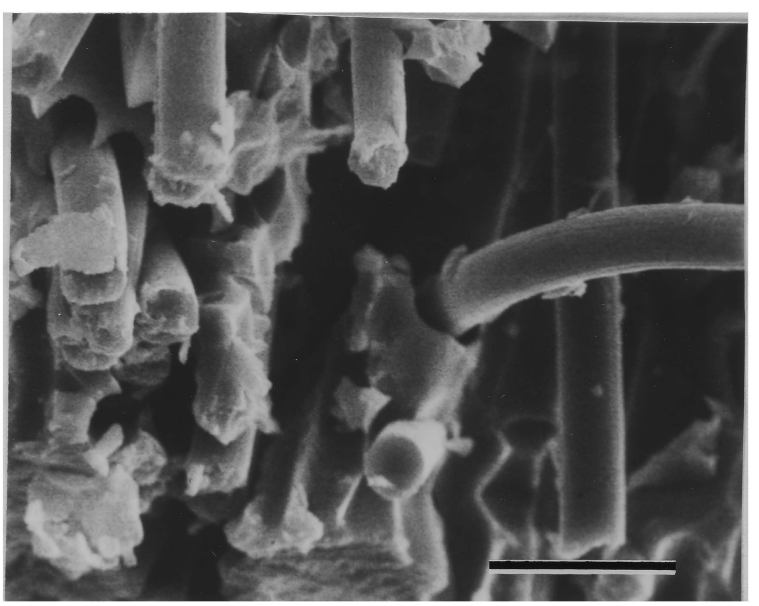

Figure 9. Scanning electron micrographs of fracture surface of carbon fiber reinforced borosilicate glass a: parallel and b: perpendicular to the fiber plane (bars = 20 micron).

surfaces parallel and perpendicular to the plane of the fibers. The preferred orientation of the fibers is evident. The generally clean fracture along the interface is indicative of the relatively low adhesion between the carbon fibers and the glass matrix.

The specimens for thermal diffusivity measurement were 8 x 10 x 2 mm rectangular plates cut from the hot-pressed billet with a slow speed precision diamond saw. Specimens were cut to permit measurement of the thermal diffusivity parallel and perpendicular to the plane of the fibers. Possible transmission of the laser beam was prevented by coating the specimens with a thin layer of colloidal carbon. The transient temperature response of the specimen rear surface was monitored by remote optical sensing, with a viewing area about 5 mm in diameter. This viewing area is sufficiently large compared to the scale of the microstructure that the detector senses the average temperature of the specimen surface. Thus complexities are avoided in evaluating the thermal diffusivity due to local surface temperature variance due to differences in the thermal conductivity and diffusivity of the fibers and the matrix [17, 18].

At greater than 600°C the composite specimens exhibited a permanent increase in thickness perpendicular to the fiber plane. This change in thickness could not be monitored while the specimens were at high temperatures. For this reason, the reported values for thermal diffusivity obtained on the heating part of the thermal cycle were based on the value of thickness of the specimens prior to heating and

adjusted for thermal expansion. The dimension of the specimens measured at room temperature following heating and cooling permitted the calculation of thermal diffusivity during the cooling part of the cycle. Preliminary observations indicated that above 600°C, the thermal diffusivity permanently decreased. To investigate this effect the samples were held at 600, 650, 675, or 700°C for about 4 hours, with data obtained during the heating, isothermal, and cooling parts of the thermal cycle.

The specific heat was determined by differential scanning calorimetry from 25 to 550 °C. The data for the thermal diffusivity, specific heat and density were used to calculate the thermal conductivity K by means of Eq. II-2. In this calculation, the decrease in density due to thermal expansion was included.

B. Results and Discussion

Figure 10 shows the thermal diffusivity for the glass matrix and the composite with heat flow parallel to the fiber plane. The specific heat data are listed in Table 2. Figure 11 shows the thermal conductivity calculated from the smooth curves drawn through the thermal diffusivity data shown in Figure 10, the specific heat and the density.

Measurement of thermal diffusivity of the composite samples at room temperature showed some scatter. For heat flow parallel to the fiber plane, 9 samples yielded a mean value of $1.77 \times 10^{-6} m^2 s^{-1}$. Maximum and minimum values were 1.82×10^{-6} and $1.72 \times 10^{-6} m^2 s^{-1}$.

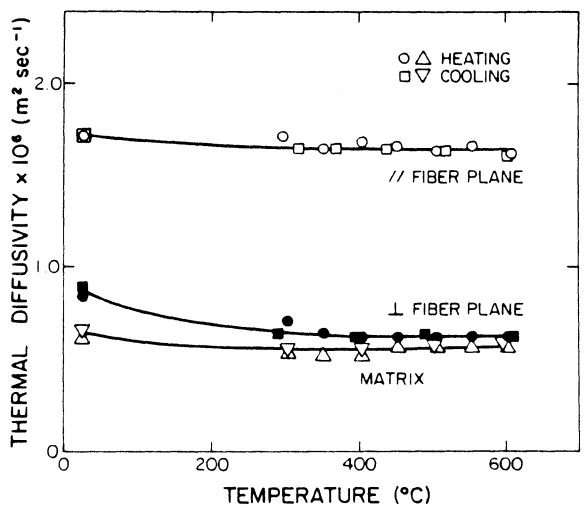

Figure 10. Effect of carbon fiber reinforcement on the thermal diffusivity of borosilicate glass.

Table 2. Specific heat ($J\ {}^{o}K^{-1}g^{-1}$) of borosilicate glass matrix and composite with carbon fibers.

Temperature (^{o}C)	Borosilicate glass	Composite with 25 vol % carbon fibers
25	0.767	0.759
100	0.872	0.898
200	0.975	1.054
300	1.066	1.161
400	1.202	1.243
500	1.255	1.325
550	1.328	1.352

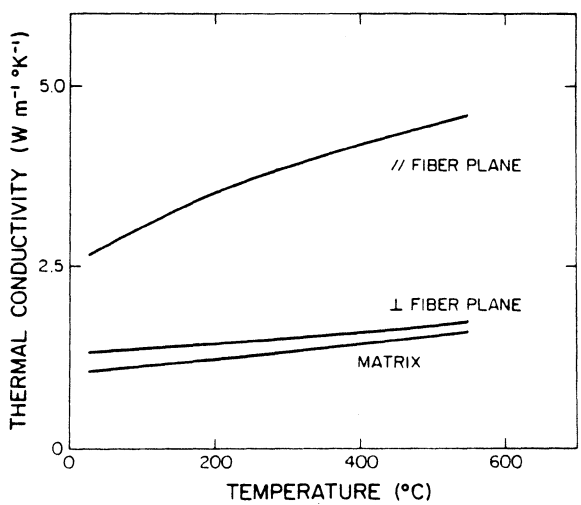

Figure 11. Effect of carbon fiber reinforcement on the thermal conductivity of borosilicate glass.

For heat flow perpendicular to the fiber plane, 7 samples had a mean value of 0.855×10^{-6} $m^2 s^{-1}$, with maximum and minimum values of 0.912×10^{-6} and $0.811 \times 10^{-6} m^2 s^{-1}$. This variation in thermal diffusivity for different samples of the composite is expected due to the small specimen size and to differences in fiber content and degree of preferred orientation from sample to sample.

The lack of temperature dependence of the thermal diffusivity of the glass as indicated by Figure 10 is typical for amorphous dielectric materials with a phonon mean free path on the order of the interatomic distances and thus not controlled by temperature-dependent phonon interactions. Lack of temperature dependence is also exhibited by the composite. This implies that the thermal diffusivity of the fibers does not vary with temperature. A variation with temperature is expected in solids with long phonon mean free paths at low temperature, and phonon mean free paths at high temperature lessened by phonon-phonon interactions. The phonon mean free path in the fibers is limited by a high density of lattice defects or regions of non-crystallinity. This is supported by the low value of Young's modulus of 235 GPa and low value of thermal conductivity parallel to the fiber axis of 15 $W\ m^{-1}\ {}^{o}K^{-1}$ at room temperature. These are less than the corresponding values for carbon fibers of 967 GPa and about 2000 $W\ m^{-1}\ {}^{o}K^{-1}$, respectively, reported by Heremans et al [19].

The coincidence of the data for the thermal diffusivity of the matrix and the composite samples obtained on heating and cooling im-

plies that over the range of 25 to 600°C, the thermal diffusivity is not affected by irreversible effects due to microstructural or compositional changes.

The data for the specific heat for the matrix and the composite are almost identical. Thus the values of specific heat of the matrix and the fibers are comparable.

The thermal conductivity data in Figure 11 suggest a number of effects. The near temperature independence of the thermal diffusivity of the matrix and composite samples for both directions of heat flow implies that the positive temperature dependence of the thermal conductivity can be attributed to the positive temperature dependence of the specific heat.

The values for the thermal conductivity of the matrix phase up to about 300°C show excellent agreement with those of Kingery [20], obtained by the direct measurement by a comparative method with specimens about 2.5 cm thick. Above 300°C the data of Kingery exceed those of the present study, by about 30% at 600°C. This difference could be attributed to a partial contribution of radiative heat transfer across the specimen to the total heat transfer through the sample. For radiative heat transfer directly across the specimen, the effective thermal conductivity increases with increasing specimen thickness. Radiative heat transfer is expected to increase with increasing temperature. For this reason, the higher values and higher temperature dependence of the data of Kingery could be attributed to

differences in specimen thickness.

For the composite, thermal conductivity normal to the fiber plane is slightly higher than that for the matrix. This suggests that for this direction of heat flow the fibers have little effect on thermal conductivity.

Heat flow within the fibers normal to the fiber axis involves heat flow normal to the graphite basal plane. In this orientation pyrolitic graphite exhibits thermal conductivity lower than in the parallel orientation [22-24].

If it is assumed that an interfacial thermal resistance is not present, an estimate of the thermal conductivity of the fibers normal to their axes can be obtained from the theory for the effective thermal conductivity for a composite in the form of a matrix with non-interacting circular cylinders oriented perpendicular to the direction of heat flow. The expression is derived for parallel circular cylinders, but if the volume fraction is sufficiently small that interaction does not occur between local temperature fields of fibers, the solution should also apply to random orientation of fibers within a plane perpendicular to heat flow. Assuming this condition is satisfied for the composites of this study, the effective thermal conductivity K_c of the composite perpendicular to the plane of the fibers is [25]:

$$K_c = K_m [(K_f/K_m - 1)V_f + 1 + K_f/K_m] / [(1-K_f/K_m)V_f + 1 + K_f/K_m] \quad \text{(IV-1)}$$

where K_m and K_f are the thermal conductivities of the matrix and fibers, respectively and V_f is the volume fraction of fibers.

With K_c = 1.3 W m^{-1} $^oK^{-1}$, K_m = 1.1 W m^{-1} $^oK^{-1}$ at 25°C as indicated by Figure 11 and V_f = 0.25, Eq. IV-1 yields K_f = 2.2 W m^{-1} $^oK^{-1}$. This value is in good agreement with 2.4 W m^{-1} $^oK^{-1}$ for as-deposited unannealed pyrolytic graphite at 25°C reported by Null et al [24]. A direct comparison may be inconclusive as the structure of the fibers, with the basal plane roughly circularly symmetric around the fiber axis, does not correspond to the planar structure of pyrolytic graphite. Heat flow in the fibers perpendicular to the fiber axis will have components parallel and normal to the basal plane. Thermal conductivity perpendicular to the fiber axis would be lower than within the graphite basal plane [20, 24].

Figures 12 and 13 show the data for the composite samples in the heating, cooling and isothermal periods of thermal cycles to 650, 675 and 700°C. In order to indicate the relative effect of temperature, the data in Figure 13 were normalized, which eliminates the effect of sample-to-sample variation in thermal diffusivity prior to heating, referred to earlier. Included in Figure 13 are the data for the samples heated to 600°C, for which heating and cooling data are presented in Figure 10. Table 3 lists the thicknesses of the samples

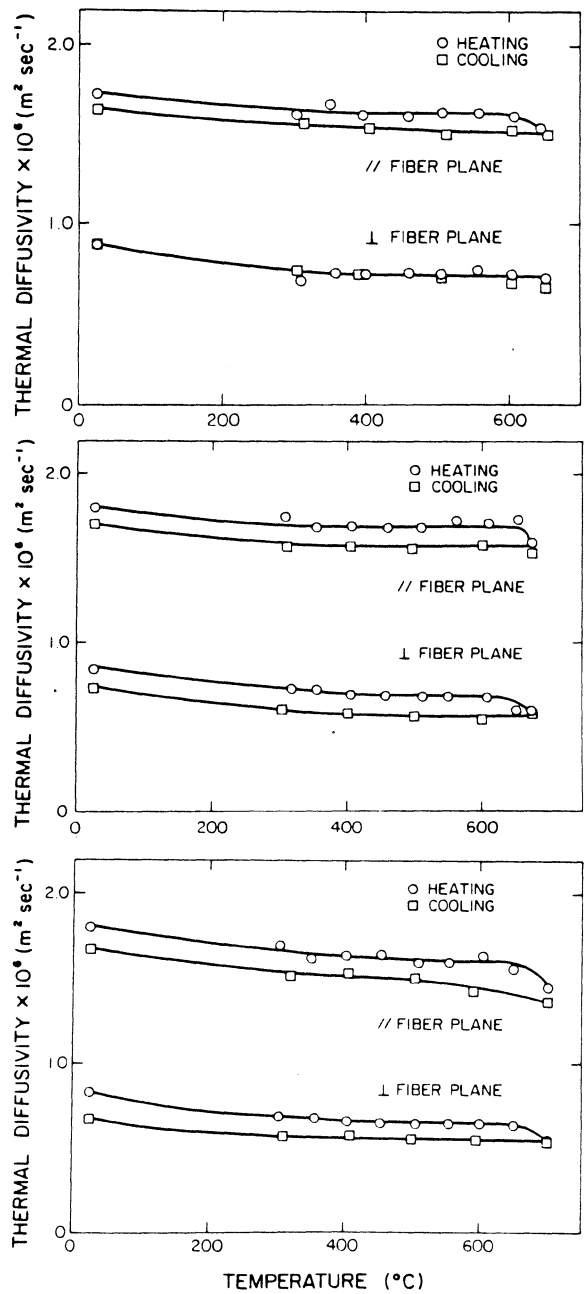

Figure 12. Thermal diffusivity of carbon fiber reinforced borosilicate glass during heating and cooling following a 4 hour anneal at a: 650°C, b: 675°C and c: 700°C.

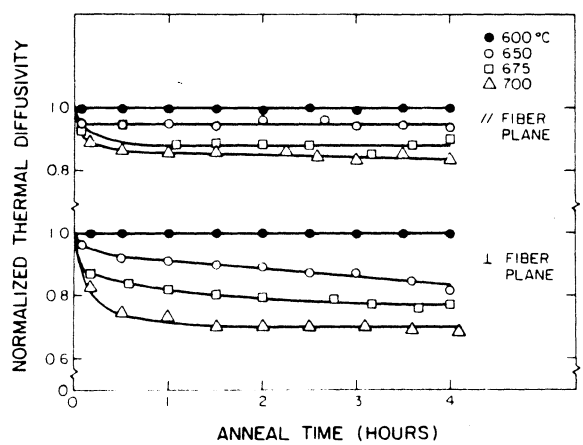

Figure 13. Relative thermal conductivity of carbon fiber reinforced borosilicate glass during 4 hour anneal at 600, 650, 675 and 700°C for the thermal cycles shown in Figures 10 and 12.

Table 3. Dimension changes of carbon fiber reinforced borosilicate glass.

Maximum Temperature of cycle (^{o}C)	Orientation with fiber plane	Thickness (cm) before	after
600	parallel	0.190	0.190
	perpendicular	0.195	0.196
650	parallel	0.203	0.203
	perpendicular	0.191	0.203
675	parallel	0.190	0.191
	perpendicular	0.195	0.208
700	parallel	0.191	0.191
	perpendicular	0.194	0.212

at room temperature prior to and following thermal cycling.

The data of Figure 12 for cycling to all three temperatures indicate a decrease in thermal diffusivity of the composites upon return to 25°C, indicative of a permanent structural change. The increase in dimensions of the specimens, which is pronounced perpendicular to the fiber plane, suggests that the structural change is the formation of voids or cavities. The data of Figure 13 suggest that the mechanism responsible for the void or cavity formation is a thermally activated process. The data of Figure 13 show that the thermal diffusivity decreases to a constant value, indicating that the structural change proceeds to a maximum limit and then ceases.

The scanning electron micrographs shown in Figure 14 of polished surfaces normal and parallel to the fiber plane show the structural change in the form of interfacial cracking between the fibers and matrix. Interfacial cracking also appeared to involve displacement of the fibers, which protruded above the surface as shown by the micrograph of the polished section parallel to the fiber plane in Fig. 14b.

The permanent structural change could originate from the elastic bending of the fibers over one another by the compaction during hot-pressing. Because the compacts were cooled while under pressure, over the lower ranges of temperature the fibers are held in place by the rigid matrix. On reheating the composites without external constraints up to a temperature sufficiently high for the matrix to undergo a change in viscosity, stress relaxation of the fibers can occur

a.

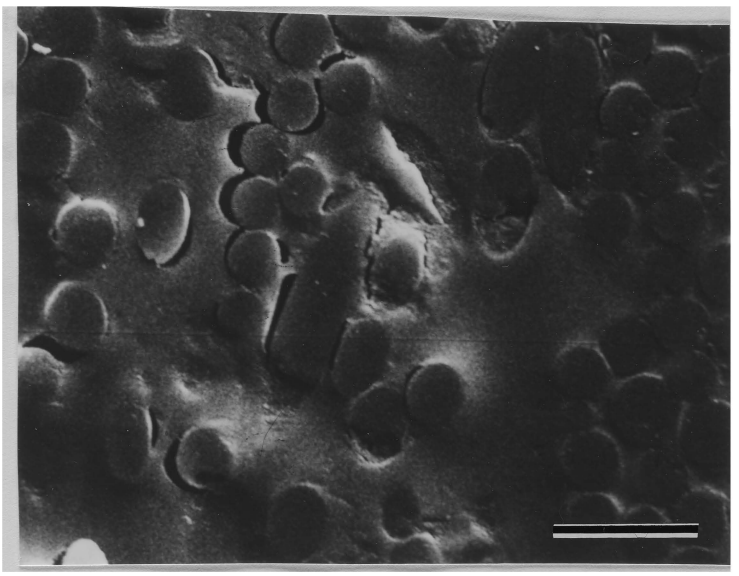

b.

Figure 14. Scanning electron micrographs of polished sections of carbon fiber reinforced borosilicate glass annealed at 650°C for 4 hours following polishing, a: parallel and b: perpendicular to the fiber plane (bars = 20 micron).

by the thermally activated viscous flow of the matrix. The viscosity data presented by McClennan and Shand [26] for Pyrex^{R} glass list the softening, annealing and strain points of 821, 560 and 510 ^{o}C, respectively. These data suggest that above 600 ^{o}C the matrix should undergo viscous deformation. The observed interfacial separation could result, leading to the lowering of thermal diffusivity.

V. CARBON FIBER - LITHIA-ALUMINOSILICATE GLASS-CERAMIC

A. Introduction

An earlier study [27] of thermal diffusivity of fiber reinforced composites showed that lithia-aluminosilicate glass-ceramic uniaxially reinforced by amorphous silicon carbide fibers had excellent thermal insulating behavior due to low thermal diffusivity of both the matrix and the silicon carbide fibers. The composite used in this study contains carbon fibers, in order to develop and characterize a composite material with the same matrix but with different properties.

B. Experimental

The matrix phase consisted of a lithia-aluminosilicate glass-ceramic with molar ratios of Li_2O, Al_2O_3 and SiO_2 of 1:1.2:6 with minor amounts of MgO and ZnO substituted for the Li_2O and TiO_2 and ZrO_2 added as nucleating agents. Crystallization was at 1000°C for 2 hours which resulted in the stuffed beta-quartz crystal structure with density of 2.50 g cm^{-3}.

The carbon fibers made by pyrolysis of polyacrylonitrile (PAN) fibers[1] were in the form of tows of yarn with about 6000 fibers per

---

[1]Hercules HMS PAN-based fibers. Young's modulus 700-800 GPa.

tow. The average fiber diameter is 7.3 micron and density is 1.877 g cm^{-3}. The crossection of the fiber is generally circularly symmetric with the basal plane of the graphite crystal structure concentric about the fiber axis.

A block of the composite was made by passing tows of yarn through a slurry of the powder of the uncrystallized glass suspended in an aqueous medium. Following drying the coated yarns were cut to length and laid parallel in a graphite die followed by hot-pressing in a nitrogen atmosphere at approximately 1300°C and 6.9 MPa. Following densification, the die was cooled to 1000°C while under pressure and held for 2 hours to assure complete crystallization. The die was then cooled to room temperature with the pressure gradually released as cooling proceeded. The fiber volume fraction of the final composite is about 30 % and density is 2.15 g cm^{-3}.

For convenience of reporting the data relative to the fiber direction, Figure 15 shows the xyz-coordinate system with the axes of the fibers coinciding with the y-axis.

Figures 16a and 16b show photomicrographs of polished sections of the composite perpendicular to the fiber direction. The inhomogeneous distribution of the fibers indicated by Figure 16a is due to the original tow form of the carbon fibers and the procedure selected by the manufacturer of the composite. Figure 16b shows an area within the composite with a relatively high fiber concentration, and indicates the penetration of matrix material between the

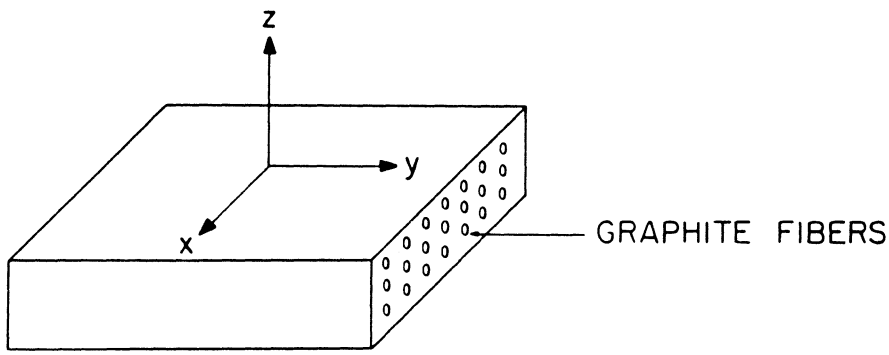

Figure 15. Orientation of carbon fiber reinforced lithia-aluminosilicate glass-ceramic.

a.

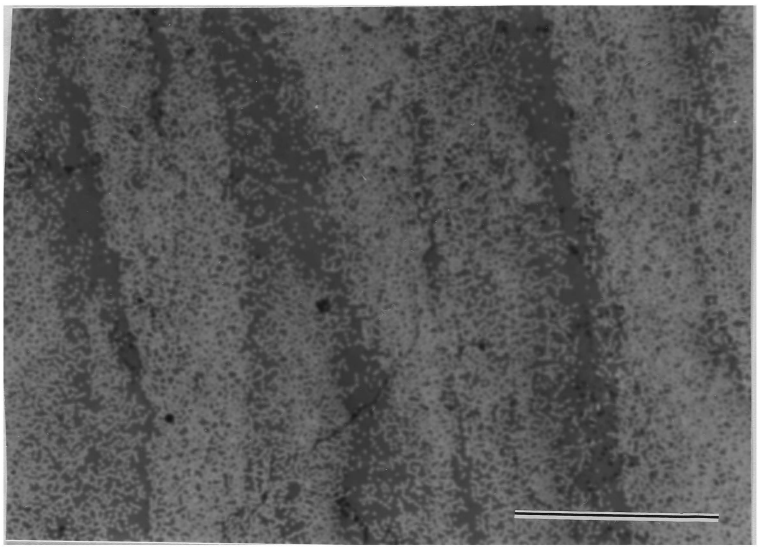

b.

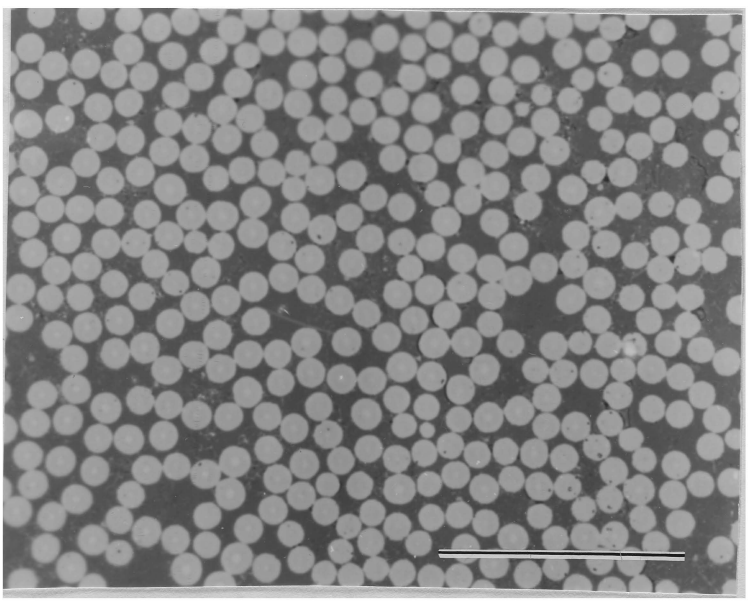

Figure 16. Optical micrographs of carbon fiber reinforced lithia-aluminosilicate glass ceramic at two magnifications, a: (bar = 500 micron) and b: (bar = 75 micron).

fibers of each tow.

Figures 17a and 17b show scanning electron micrographs of fracture surfaces perpendicular and parallel to the fiber direction, respectively. The clean fracture along the interface indicates a low degree of adhesion between the fibers and the matrix. Some ares of separation between the fibers and the matrix are evident.

The specimens for these measurements were 8 x 10 x 2mm rectangular plates cut from the hot-pressed billet with a slow speed precision diamond saw. Possible transmission of the laser beam was prevented by coating the specimens with a thin layer of colloidal colloidal carbon. The transient temperature response of the specimen rear surface was monitored by remote optical sensing, with a viewing area on the specimen about 5 mm in diameter. This viewing area is sufficiently large compared to the scale of the microstructure that the detector senses the average temperature of the specimen surface, and complexities are avoided in evaluating the thermal diffusivity due to local surface temperature differences caused by differences in the thermal conductivity and diffusivity of the fibers and the matrix [17, 18].

Preliminary data indicated that for heat flow perpendicular to the fiber direction a permanent decrease in thermal diffusivity resulted. This also was found to be a function of the maximum temperature. For this reason, measurements were made over two successive cycles up to approximately 350, 600 and 1000^{o}C. Data were also obtained for one

a.

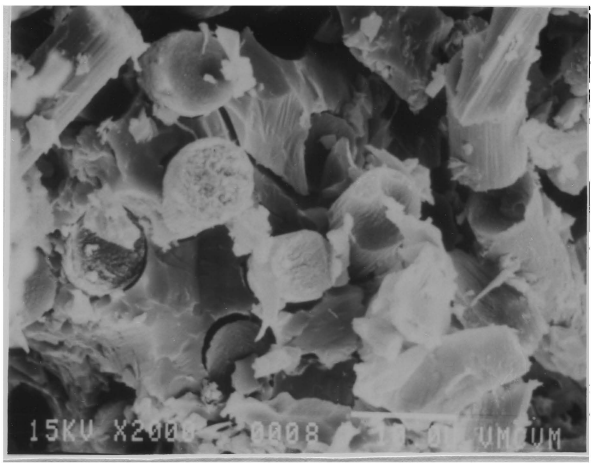

b.

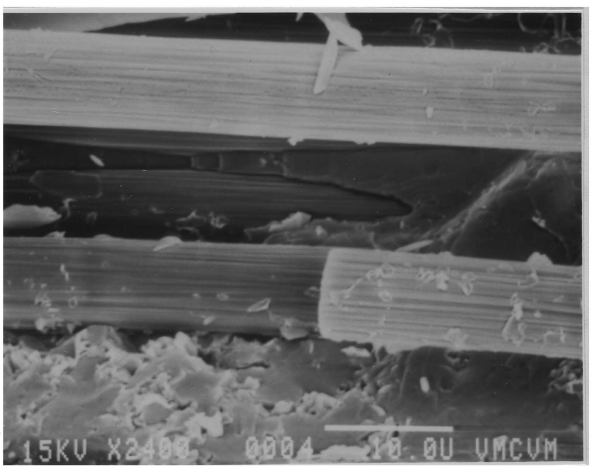

Figure 17. Scanning electron micrographs of fracture surfaces of carbon fiber reinforced lithia-aluminosilicate glass-ceramic, a: parallel (bar = 10 micron) and b: perpendicular (bar = 10 micron) to the fiber direction.

specimen held at approximately 300°C for about 4 hours.

The specific heat was determined by differential scanning calorimetry from room temperature to 600°C. The combined data for the thermal diffusivity, specific heat and density were used to calculate thermal conductivity using Eq. II-2.

C. Results and Discussion

Figure 18 shows the experimental data for thermal diffusivity at room temperature as a function of specimen thickness for the LAS matrix and for the x, y and z directions for the composite material. These data indicate that the value for the thermal diffusivity of the composite in the y-axis parallel to the fiber direction is much higher than in the x- and z-directions and also much higher than the corresponding value of the matrix phase. Such differences in thermal diffusivity can be attributed to two effects. As indicated by the theory [14] for the thermal conductivity of composites with components of isotropic material symmetry, thermal conductivity parallel to the fiber direction is the maximum value (upper bound) for a composite, regardless of the values of the thermal conductivities of the components. In the present case, a contributing factor to the higher thermal diffusivity in the y-direction is that the axes of the fibers coincide with the graphite basal plane. The fibers are not isotropic, and the basal plane of pyrolitic graphite [22-24] coincides with the two directions of maximum thermal conductivity and diffusivity in the graphite crys-

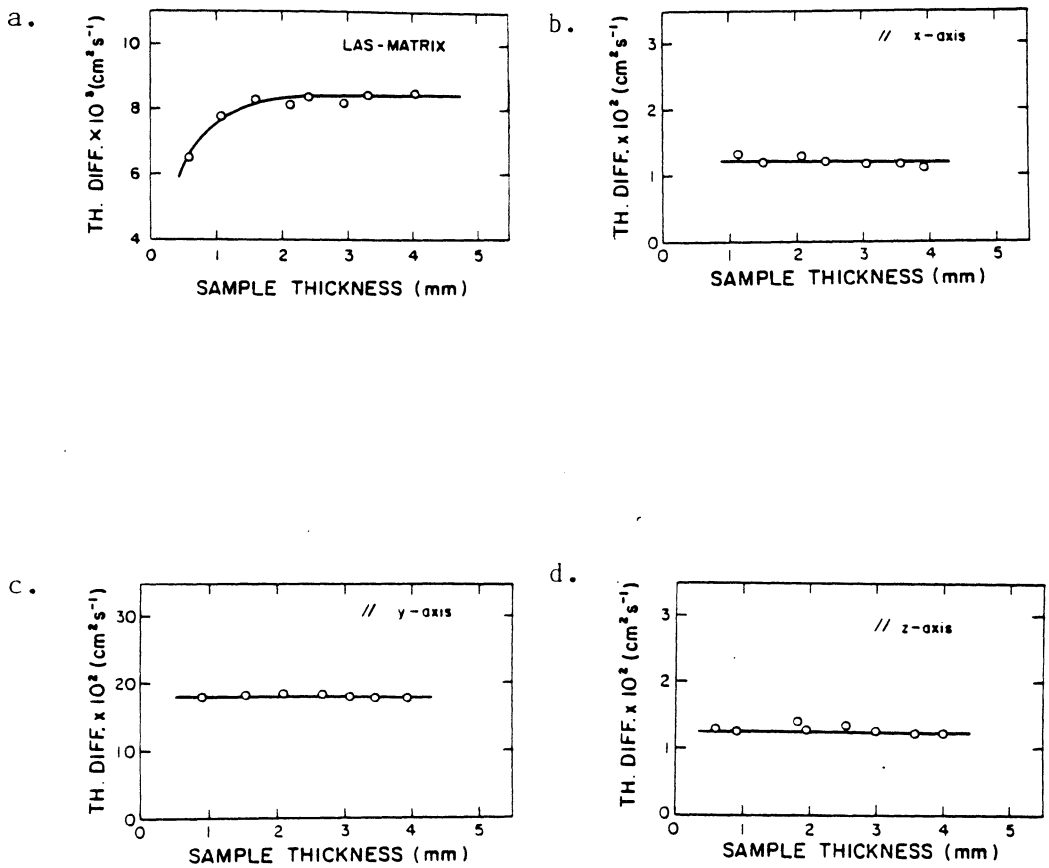

Figure 18. Dependence of thermal diffusivity at 25°C on specimen thickness for a: lithia-aluminosilicate glass-ceramic and b, c, d: carbon fiber reinforced lithia-aluminosilicate glass-ceramic.

tal structure. Perpendicular to this plane, the thermal conductivity and thermal diffusivity can be less by as much as several orders of magnitude. For this reason, for heat flow perpendicular to the fiber direction, the presence of the fibers is expected to have a smaller effect on the thermal diffusivity, as observed. In the x- and z-directions the thermal diffusivity is increased by less than a factor of two over the value of the matrix. As will be shown later, perpendicular to the fiber direction, the heat conduction appears also to be affected by the presence of an interfacial thermal resistance.

The data in Figure 18 indicate a specimen size effect on the thermal diffusivity of the matrix but the absence of such an effect in the composite in all three directions. This agrees with findings in earlier studies [24, 27]. The existence of a size effect indicates a contribution of radiative heat transfer through the specimen to the total thermal conductivity. The absence of a size effect on the thermal diffusivity in all three directions within the composite can be attributed to the high value of the absorption coefficient of the carbon fibers which effectively suppresses the radiative contribution to the total heat conduction.

Figure 19 shows the temperature dependence of the thermal diffusivity of the LAS matrix up to 900°C for a specimen with thickness of 1.97 mm. This is outside of the range of thickness for which the thermal diffusivity is dependent on thickness as shown in Figure 18a. Up to about 400°C, the data in Figure 19 show a negative temperature

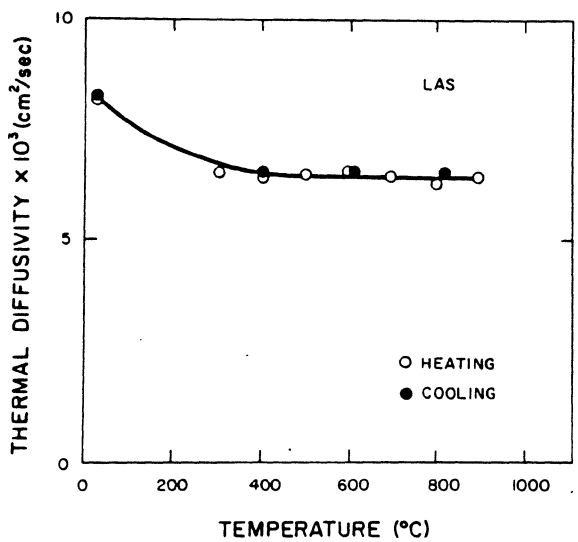

Figure 19. Temperature dependence of thermal diffusivity of lithia-aluminosilicate glass-ceramic.

dependence as expected for a dielectric crystalline solid in which heat is conducted primarily by phonons. Above 400°C, the thermal diffusivity appears to be independent of temperature, probably due to a contribution of radiation, which increases with increasing temperature. The positive temperature dependence of the radiation heat transfer could offset the negative temperature dependence of the phonon heat transfer, resulting in little variance with temperature of the total heat transfer.

The data coincide on heating and cooling, indicating that over the temperature span involved the specimen did not undergo any structural or compositional change which would affect heat transfer.

Figure 20 shows the experimental data for thermal diffusivity of the composite along the y-axis, parallel to fibers, as a function of temperature for two samples heated to 600 or 1000°C. These data indicate a negative temperature dependence of the thermal diffusivity over the total range of temperature. The data obtained on heating or cooling are identical within experimental error. On remeasurement of the thermal diffusivity over subsequent thermal cycles, the data were identical within the experimental error. These observations suggest for heat flow parallel to the fiber axis, the thermal diffusivity is not affected by permanent structural or compositional changes in the fiber or matrix phase.

Figures 21a, 21b and 21c show the data for the thermal diffusivity along the x-axis for separate specimens heated to and cooled from

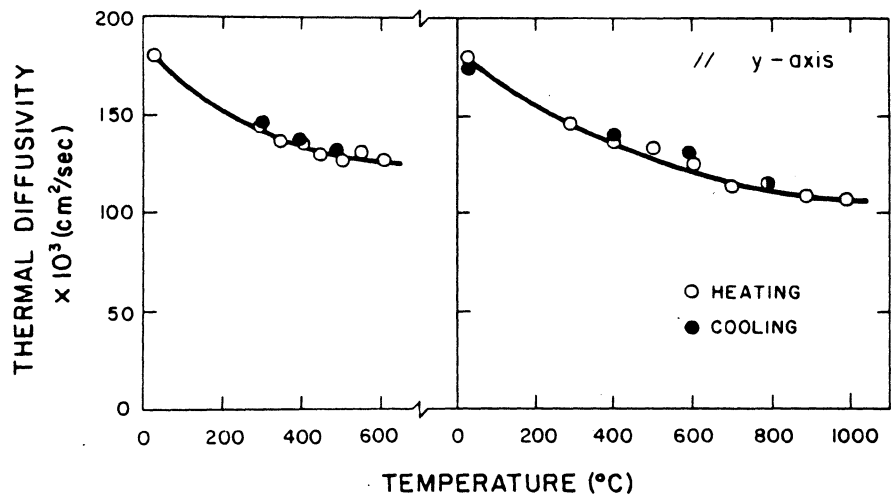

Figure 20. Temperature dependence of thermal diffusivity of carbon fiber reinforced lithia-aluminosilicate glass-ceramic parallel to the fiber direction.

a.

b.

c.

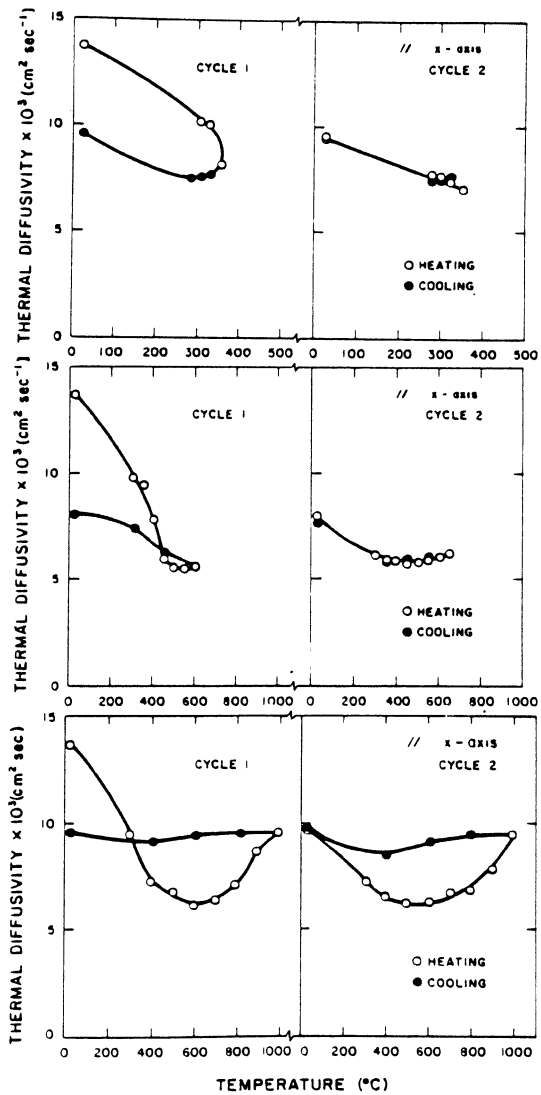

Figure 21. Temperature dependence of thermal diffusivity of carbon fiber reinforced lithia-aluminosilicate glass-ceramic to a: 350°C, b: 600°C and c: 1000°C.

about 350, 600 and 1000°C, respectively, over two successive thermal cycles. The data for heat flow in the z-direction were essentially identical to those in the x-direction. The data for subsequent cycles were identical to those of the second cycle within experimental error.

The data in Figure 21 indicate a different relative dependence of the thermal diffusivity on temperature compared to the data shown in Figure 20. Two effects appear to opere for heat flow perpendicular to the fiber direction. On heating during the first cycle the thermal diffusivity undergoes a permanent decrease. During the second cycle on heating to and cooling from 1000°C, the thermal diffusivity exhibits a hysteresis, with the data on cooling exceeding the data on heating.

The permanent decrease in thermal diffusivity during the first cycle may be attributed to the formation of structural discontinuities which inhibit heat conduction. As shown in Figure 22, this decrease in thermal diffusivity was time dependent during an isothermal anneal at 300°C for 4 hours.

In Figure 23 optical microscopy of a polished 8 x 2 mm side surface of the specimen used for the generation of the data in Figure 22 revealed the formation of cracks following the 4 hour anneal at 300°C. The cracks were not present prior to the anneal. As indicated by Figure 23, the cracks form perpendicular to the surface and parallel to the fiber direction. It appears that wherever possible the fiber-matrix interface was the preferred path of crack

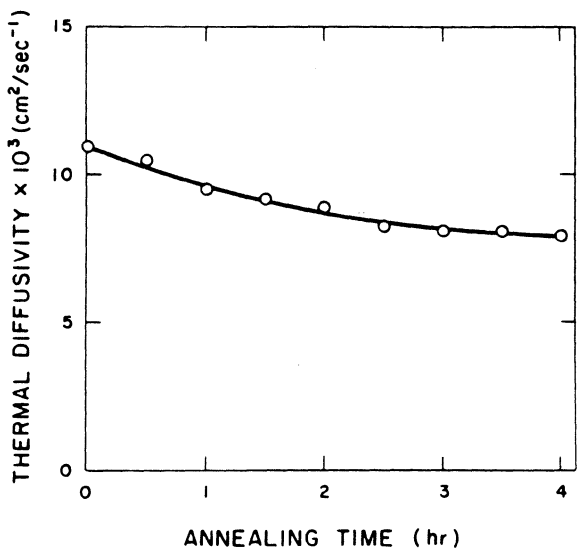

Figure 22. Time dependence of thermal diffusivity of carbon fiber reinforced lithia-aluminosilicate glass-ceramic perpendicular to the fiber direction at 300°C.

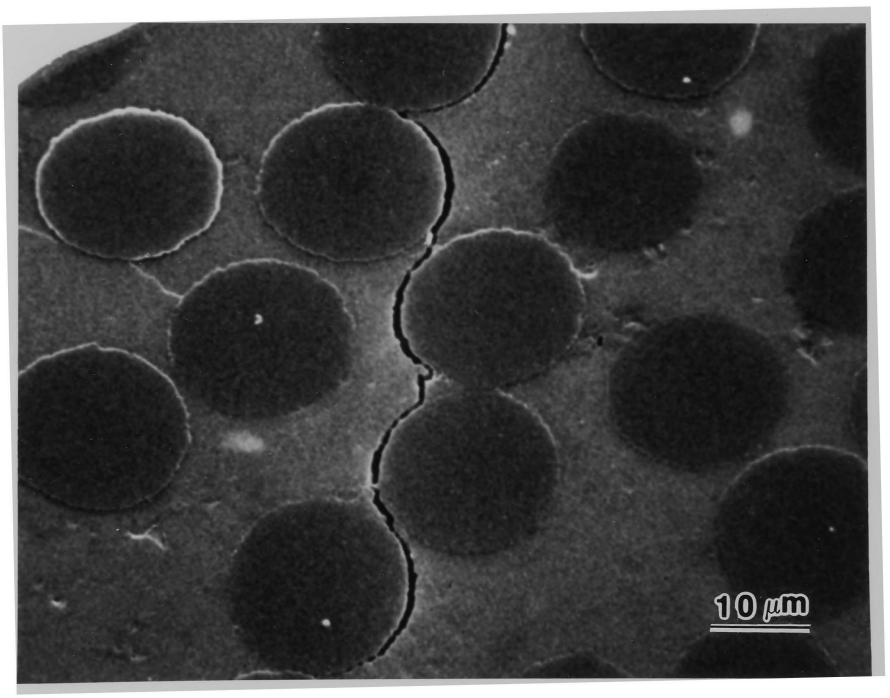

Figure 23. Crack in carbon fiber reinforced lithia-alumino-silicate glass-ceramic following anneal at 1000°C for 4 hours.

propagation. Such fracture along the interface would be promoted by incomplete adhesion between the matrix and the fibers. Cracks have been shown to be effective in lowering thermal conductivity [24]. The permanent decrease in thermal diffusivity during the first thermal cycle is probably due to the formation of cracks.

The permanent cracking shown in Figure 23 suggests that residual stresses provide the driving force for crack formation. In an earlier study [29], crack formation represented a possible mechanism for residual stress relief. In the present composites, residual stresses can arise from a number of sources. A thermal expansion mismatch exists between the fibers and matrix, with the coefficient of thermal expansion perpendicular to the fiber axis of $18 \times 10^{-6}\ ^{o}C^{-1}$, and the corresponding value for the matrix less than $1 \times 10^{-6}\ ^{o}C^{-1}$. The direction of this mismatch upon cooling from the crystallization temperature resulted in radial tensile stresses within the fibers, at the interfaces and in the matrix immediately surrounding the fibers. Such radial stresses could promote interfacial fracture and separation. Other stresses may have existed due to the anisotropic symmetry of the fibers. Internal stresses which arose on cooling to ambient temperature from spatially nonuniform temperatures during hot-pressing and crystallization are a possible further cause of crack formation. These stresses are expected to exist within large regions of the composite and can result in cracks which could propagate along many neighboring fibers as shown in Figure 23.

The approximately 6% decrease in volume of the glass-ceramic during crystallization is expected to result in internal stresses of high magnitude and could be the primary reason for the formation of the cracks shown in Figure 23.

A hysteresis in thermal diffusivity on heating and cooling is evident on heating to 1000°C and absent on heating to 350 and 600°C, as shown in Figure 21. This is possibly related to a thermal history dependent thermal resistance at the fiber-matrix interface, due to a thermal expansion mismatch between the matrix and fibers normal to the fiber direction. If so, the temperature dependence of the thermal diffusivity of the composite should be determined by the temperature dependence of the thermal diffusivity of the fibers, the matrix and the interface. The data in Figure 21 suggest qualitatively that up to approximately 600°C the negative temperature dependence of the thermal diffusivity of the composite is controlled by the negative temperature dependence of the thermal diffusivity of the matrix and the fibers. Between 600°C and 1000°C, the effectiveness of the interfacial thermal resistance decreases with increasing temperature. This results in an increase in the thermal diffusivity of the composite with increasing temperature upon heating from 600°C to 1000°C.

If the magnitude of the interfacial thermal resistance was a function only of the temperature, the thermal diffusivity at any temperature would be independent of thermal history. The existence of a hysteresis in thermal diffusivity on heating to and cooling from

1000°C suggests that the thermal resistance is a function of both thermal history and temperature.

Figure 24 shows the data for the specific heat of the matrix with and without the 30 vol % carbon fibers. These data show that the specific heat of the composite is less than that of the matrix. This is to be expected because the specific heat of graphite or diamond [30] is less than that of the matrix within the temperature range of this study.

The values of thermal conductivity which correspond to the experimental data for the thermal diffusivity can be calculated by Eq. II-2 taking into account the changes in density due to thermal expansion. Because the specific heat and density are scalar quantities, the data for thermal conductivity for different directions of heat flow and different thermal histories at any temperature will show the same quantitative difference. As a result of the increase in the specific heat with increasing temperature, the thermal conductivity will exhibit a more positive temperature dependence than the thermal diffusivity.

For evaluating the thermal conductivity of the fibers parallel to their axes, Figure 25 shows the calculated values of the thermal conductivity from 25°C to about 600°C for the matrix with and without the carbon fibers, calculated from the smooth curve drawn through the data for the thermal diffusivity shown in Figures 19 and 20. The matrix shows a positive temperature dependence of thermal

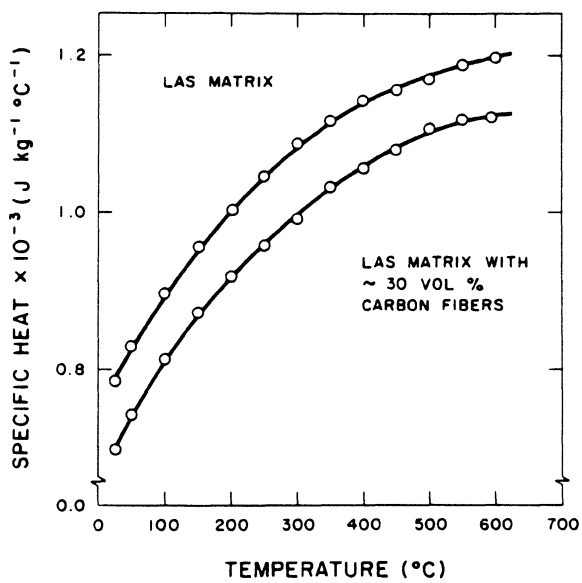

Figure 24. Effect of carbon fiber reinforcement on the specific heat of lithia-aluminosilicate glass-ceramic.

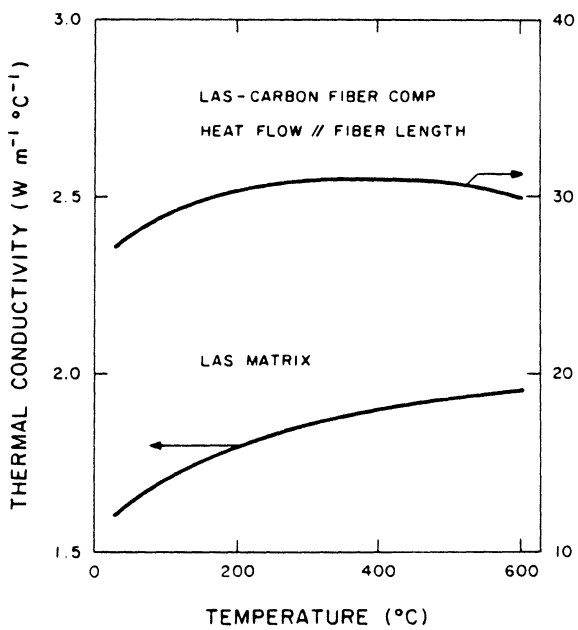

Figure 25. Effect of carbon fiber reinforcement on the thermal conductivity of lithia-aluminosilicate glass-ceramic.

conductivity over the total temperature range. This effect arises because as temperature increases, the relative increase of the specific heat is greater than the relative decrease of the thermal diffusivity. A similar positive temperature dependence is exhibited by the composite, except at the higher temperatures, at which the thermal conductivity exhibits a slight negative temperature dependence. Because of the negative temperature dependence of polycrystalline graphite [31] and pyrolytic graphite along the basal plane [22-24], it was expected that the thermal conductivity of the composite would exhibit a negative temperature dependence as well. A partial answer to this apparent discrepancy can be provided by an estimate of the thermal conductivity of the fibers.

For a two component uniaxial fiber reinforced composite with heat flow along the fibers, the effective thermal conductivity is:

$$K_c = K_1V_1 + K_2V_2 \qquad \text{(V-1)}$$

where K is the thermal conductivity, V is the volume fraction and the subscripts c, 1 and 2 refer to the composite, matrix and fibers, respectively. Figure 25 shows that at room temperature, K_c = 27 W m^{-1} $^oK^{-1}$ and K_1 = 1.6 W m^{-1} $^oK^{-1}$. For V_2 = 30 vol %, Eq. II-1 yields for the thermal conductivity of the fibers in the axial direction K_2 = 90 W m^{-1} $^oK^{-1}$. This is much less than the values of 306 and 1840 W m^{-1} oK-1 for as-deposited and annealed pyrolytic graphite, respectively, within the basal plane at room temperature as

found by Null et al [24] and others [28-31], but compares well with the value of 150 W m^{-1} $^{o}K^{-1}$, found by Heremans et al [19] and 175 W m^{-1} $^{o}K^{-1}$ found by Nysten et al [32], by the direct measurement of the thermal conductivity of PAN-based carbon fibers. These low values for thermal conductivity and associated small temperature dependence are attributed to the high concentration of lattice defects and incomplete graphitization of the PAN-based carbon fibers [36].

VI. EFFECTIVE THERMAL CONDUCTIVITY OF COMPOSITES WITH INTERFACIAL THERMAL RESISTANCE

A. Introduction

The effective thermal conductivity of composite materials has been a topic of theoretical interest, as have other transport properties [25, 37-48]. Generally, it has been found that the effective thermal conductivity is a function of the component thermal conductivities, their geometric distribution and their volume fraction, but not of their dimensions. Recent experimental results [45, 46] for the thermal diffusivity of composites consisting of spherical nickel dispersions in a glass matrix and of carbon fiber reinforced glass-ceramic indicated that the effective thermal conductivity can be affected by thermal resistance at the interface between phases. In the cited studies [3, 49] the thermal resistance arises from poor mechanical or chemical adhesion at the interface and mismatch in coefficients of thermal expansion. Upon cooling from manufacturing temperature, a gap formed between the phases. The data for thermal diffusivity indicated that the interfacial thermal resistance of the gap lowered the effective thermal conductivity and thermal diffusivity by a factor of two in the nickel-glass system [49].

The effect of interfacial barriers on conductive properties was the subject of earlier studies of the effective thermal conductivity of single phase materials with cracks [28, 50] and two layer plate composites [51] and the electrical conductivity of insulating matrices with conductive dispersed phases [52-54].

A literature search indicated that no theories appear to have been

developed for the effective thermal conductivity of matrices with dilute volume fraction of dispersions and a thermal barrier at the interfaces.

Expressions for the effect of an interfacial thermal resistance on the effective thermal conductivity of composites with spherical or cylindrical dispersed phase geometry can be obtained by a minor modification of the original Rayleigh and Maxwell theories [25, 37]. For flat plate geometry with heat flow perpendicular to the plates, a solution can be obtained by a series resistance model.

B. Analysis

Dispersions with thermal conductivity K_d are in a matrix with thermal conductivity K_m. The volume fraction of dispersions V_d is assumed sufficiently dilute that interactions between the temperature fields of neighboring dispersions are absent. The interfacial thermal resistance is expressed as a boundary conductance, h_c.

1. Spherical Dispersions

The temperature T_d within the spherical dispersion of radius a and the temperature T_m in the surrounding matrix are assumed to be of the form:

$$T_d = rA(\cos\theta) \qquad \text{(VI-1a)}$$

$$T_m = (\nabla T)r(\cos\theta) + (B/r^2)(\cos\theta) \qquad \text{(VI-1b)}$$

where ∇T is the temperature gradient at large distances from the dispersion, A and B are constants to be solved and r and θ are spherical coordinates with θ the angle between the radius vector r and the temperature gradient.

Boundary conditions for Equations VI-1a and VI-1b at r = a:

$$K_d \left(\partial T_d/\partial r\right) = K_m \left(\partial T_m/\partial r\right) \qquad \text{(VI-2a)}$$

$$T_d - T_m = -(K_d/h_c)(\partial T_d/\partial r) \qquad \text{(VI-2b)}$$

In the absence of an interfacial thermal resistance ($h_c = \infty$) Eq. VI-2a becomes:

$$T_d = T_m \qquad (r=a) \qquad \text{(VI-2c)}$$

which is the boundary condition for the derivation by Maxwell [37].

Solving for A and B and substitution into Eq. VI-1 yields:

$$T_d = (\nabla T) r(\cos\theta) \frac{\left[1 + \left[\frac{K_m}{ah_c} + \frac{K_m}{K_d} - 1\right]\left[1 + \frac{2K_m}{K_d}\left[\frac{K_d}{ah_c} + 1\right]\right]^{-1}\right]}{\left[\frac{K_d}{ah_c} + 1\right]} \qquad \text{(VI-3a)}$$

$$T_m = (\nabla T) r(\cos\theta) + \frac{(\nabla T) r(\cos\theta) a^3}{r^2} \frac{\left[\frac{K_m}{ah_c} + \frac{K_m}{K_d} - 1\right]}{\left[1 + \frac{2K_m}{K_d}\left[\frac{K_d}{ah_c} + 1\right]\right]} \qquad \text{(VI-3b)}$$

For $h_c = \infty$, Eqs. VI-3a and VI-3b become:

$$T_d = (\nabla T) r \cos\theta \left[\frac{3K_m}{K_d + 2K_m}\right] \qquad \text{(VI-4a)}$$

$$T_m = (\nabla T) r(\cos\theta) + \frac{(\nabla T) r(\cos\theta)\, a^3}{r^2} \frac{(K_m - K_d)}{(2K_m + K_d)} \qquad \text{(VI-4b)}$$

in agreement with Maxwell [37].

The derivation of the effective thermal conductivity of the composite relies on assessing the effect on T_m of n spheres of radius a within a large sphere of radius b, which has effective thermal conductivity K_{eff}.

In terms of n spheres of radius a, Eq. VI-3b becomes:

$$T_m = (\nabla T) r(\cos\theta) + \frac{(\nabla T) r(\cos\theta)\, n a^3}{r^2} \frac{\left[\frac{K_m}{a h_c} + \frac{K_m}{K_d} - 1\right]}{\left[1 + \frac{2K_m}{K_d}\left[\frac{K_d}{a h_c} + 1\right]\right]} \qquad \text{(VI-5a)}$$

which in terms of the sphere of radius b and thermal conductivity K_{eff} becomes:

$$T_m = (\nabla T) r(\cos\theta) + \frac{(\nabla T) r(\cos\theta)\, b^3}{r^2} \frac{\left[\frac{K_m}{bh_c} + \frac{K_m}{K_{eff}} - 1\right]}{\left[1 + \frac{2K_m}{K_{eff}}\left[\frac{K_{eff}}{bh_c} + 1\right]\right]} \qquad \text{(VI-5b)}$$

The last terms in Eqs. VI-5a and VI-5b must be equal. With $V_d = na^3/b^3$ and for b very large such that $K_m/bh_c = K_{eff}/bh_c = 0$, this yields:

$$K_{eff} = K_m \frac{2\left[\frac{K_d}{K_m} - \frac{K_d}{ah_c} - 1\right] V_d + \frac{K_d}{K_m} + \frac{2K_d}{ah_c} + 2}{\left[1 - \frac{K_d}{K_m} + \frac{K_d}{ah_c}\right] V_d + \frac{K_d}{K_m} + \frac{2K_d}{ah_c} + 2} \qquad \text{(VI-6)}$$

For $h_c = \infty$, Eq. VI-6 agrees with the expression of Maxwell [37] for K_{eff} without an interfacial thermal resistance.

2. Circular Cylinders Perpendicular to Heat Flow.

The temperature T_p within the circular cylindrical dispersions of radius a and the temperature T_m in the matrix were assumed to be described by:

$$T_d = rA\cos\theta \tag{VI-7a}$$

$$T_m = (\nabla T)\, r\cos\theta + (B/r)\cos\theta \tag{VI-7b}$$

where r and θ represent a circular coordinate system.

Eqs. VI-7a and VI-7b are subject to the boundary conditions given by Eqs. VI-2a and VI-2b. Solving for A and B yields:

$$T_d = (\nabla T) r(\cos\theta)\, \frac{\left[1 + \left[\frac{K_m}{K_d} + \frac{K_m}{ah_c} - 1\right]\left[\frac{K_m}{K_d} + \frac{K_m}{ah_c} + 1\right]^{-1}\right]}{1 + \frac{K_d}{ah_c}} \tag{VI-8a}$$

$$T_m = (\nabla T) r(\cos\theta) + \frac{(\nabla T) r(\cos\theta)\, a^2}{r}\, \frac{\left[\frac{K_m}{K_d} + \frac{K_m}{ah_c} - 1\right]}{\left[\frac{K_m}{K_d} + \frac{K_m}{ah_c} + 1\right]} \tag{VI-8b}$$

For $h_c = \infty$, Eqs. VI-8a and VI-8b become:

$$T_d = (\nabla T) r(\cos\theta) \quad \frac{2K_m}{(K_m + K_d)} \tag{VI-9a}$$

$$T_m = (\nabla T) r(\cos\theta) + \frac{(\nabla T)\, r(\cos\theta) a^2}{r} \quad \frac{(K_m - K_d)}{(K_m + K_d)} \tag{VI-9b}$$

which are in agreement with the solutions of Rayleigh [25].

There are assumed n cylinders within a circular area normal to the cylinder axes and of radius b, with b >> a. The effect of the cylinders on the temperature distribution within the circular area can be considered and the effective thermal conductivity K_{eff} can be obtained in a similar way as K_{eff} for spherical inclusions. Assuming b is very large such that $K_m/bh_c = 0$, K_{eff} becomes:

$$K_{eff} = K_m \frac{\left[\frac{K_d}{K_m} - 1 - \frac{K_d}{ah_c}\right] V_d + 1 + \frac{K_d}{ah_c} + \frac{K_d}{K_m}}{\left[1 + \frac{K_d}{ah_c} - \frac{K_d}{K_m}\right] V_d + 1 + \frac{K_d}{ah_c} + \frac{K_d}{K_m}} \tag{VI-10}$$

For $h_c = \infty$, Eq. VI-10 agrees with the solution of Rayleigh [25].

3. Flat Plates Perpendicular to Heat Flow.

The composite consists of a matrix with parallel flat plate dispersions with thickness, a, oriented perpendicular to heat flow, with n the concentration of dispersions per unit volume. The volume fraction V_d is:

$$V_d = na \tag{VI-11}$$

By considering the composite equivalent to a series circuit, the effective thermal resistivity (K^{-1}_{eff}) is obtained by summing the thermal resistivity of each component plus the interfacial thermal resistances. There are 2 interfaces for each plate or 2n per unit volume.

The thermal resistivity of the composite brcomes:

$$1/K_{eff} = V_d/K_d + (1 - V_d)/K_m + 2n/h_c \tag{VI-12}$$

which considering Eq (VI-11) and rearranging yields:

$$K_{eff} = \frac{K_d}{1 - \frac{K_d}{K_m} + \frac{2K_d}{ah_c} V_d + \frac{K_d}{K_m}} \tag{VI-13}$$

For $h_c = \infty$, this can be written:

$$1/K_{eff} = V_d/K_d + V_m/K_m \qquad \text{(VI-14)}$$

in agreement with the lower bound on the thermal conductivity of a two-component composite with zero contact resistance [54].

4. Discussion

The results indicate that the effect of the interfacial thermal resistance on the effective thermal conductivity is controlled by the non-dimensional parameter K_d/ah_c and its value relative to the ratio K_d/K_m. Figure 26 illustrates the effective thermal conductivity as a function of volume fraction for spherical dispersions with $K_d/K_m = 10$ and values for K_d/ah_c ranging from 0 to infinity. For $K_d/ah_c = \infty$ ($h_c = 0$) the effective thermal conductivity equals that for a matrix with a dispersed pore phase of zero thermal conductivity, regardless of the value of K_d.

Because the value of K_d/ah_c depends on the dimensions of the dispersions, the effective thermal conductivity for a composite with a value of h_c not equal to infinity will depend on the size and distribution of the dispersed phase. A size effect is not predicted by the theory for the thermal conductivity of composites with perfect thermal contact

Hatta and Taya [48] developed a theory for the effective thermal conductivity of composites with coated dispersions. A value of thermal

conductivity of the coating less than for the matrix represents a thermal resistance. The theory of Hatta and Taya does not predict the effect of dispersion size. Their theory should be valid for high values of volume fractions of dispersions while the present theory is valid only for dilute volume fractions of the dispersions.

A condition is encountered for the flat-plate geometry for which $K_{eff} \rightarrow 0$ as $h_c \rightarrow 0$, regardless of the values of K_d and K_m. This is not the case for dispersions of spherical or cylindrical geometry, so that flat plate geometry with heat flow normal to the plates is most effective in lowering the thermal conductivity for $h_c \rightarrow 0$.

Interfacial thermal barriers are expected to be effective only if they are nonparallel to the direction of heat flow. For nonspherical dispersions with preferred orientation, an interfacial thermal resistance can serve as a mechanism for introducing anisotropy in thermal conductivity even when $K_d = K_m$.

The above analysis can be extended to more complex dispersed phase geometries and higher volume fractions. Although this analysis was presented in terms of thermal conductivity, the results are applicable to other composite properties which involve flow or flux, such as electrical conductivity and dielectric and magnetic properties.

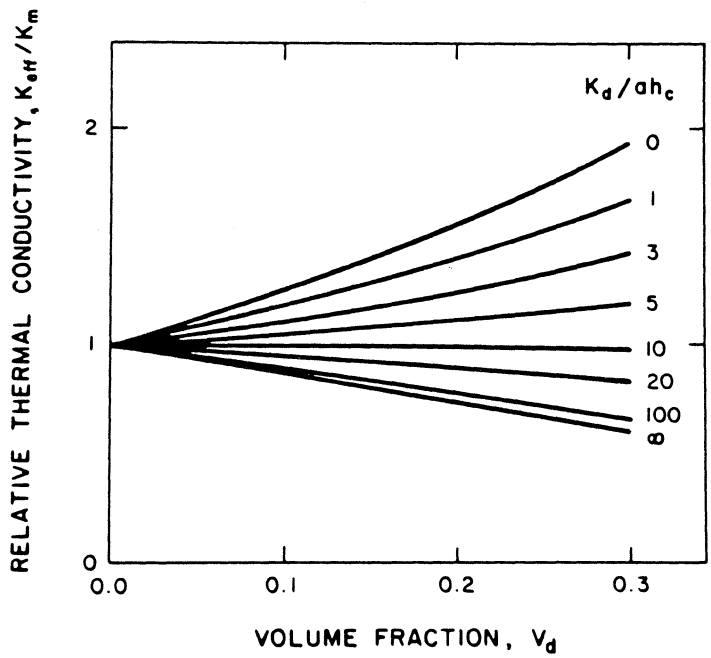

Figure 26. Effective thermal conductivity of matrix with spherical dispersions for $K_d/K_m = 10$ and a range of values of K_d/ah_c.

VII. CONCLUSION

The foregoing results have demonstrated that the thermal diffusivity and thermal conductivity of ceramic composites can be determined experimentally, and several variables which affect these properties have been identified.

The thermal diffusivity and thermal conductivity of Ba-osumilite glass-ceramic were compared to those of SiC whisker reinforced Ba-osumilite and SiC fiber reinforced Ba-osumilite. The thermal diffusivity and thermal conductivity of the SiC whisker composite are greatly influenced by the respective properties of the SiC whiskers and the whisker orientation. The whiskers preferentially align normal to the hot-pressing direction. The thermal diffusivity and thermal conductivity within the plane of preferred alignment are significantly higher than in the transverse direction. The thermal diffusivity and thermal conductivity of the whisker composites are high at 25°C, then decrease greatly with increasing temperature, influenced by the temperature dependence of the SiC whiskers. The thermal diffusivity and thermal conductivity of the SiC fiber reinforced Ba-osumilite are close to those of the glass-ceramic over the temperature range of measurement. This indicates that the thermal diffusivity and thermal conductivity of the SiC fibers are about the same as those of the Ba-osumilite glass-ceramic.

The thermal diffusivity and thermal conductivity are affected

by the orientation of the fibers in a carbon fiber reinforced borosilicate glass. Within the plane of randomly oriented chopped fibers, the thermal diffusivity and thermal conductivity are significantly higher than in the transverse direction. Thermal diffusivity normal to the fiber plane exhibited a permanent decrease above 600°C. This is caused by cavity formation as fibers, which were elastically bent and then constrained by the matrix during processing, flex to their original shape as the viscosity of the matrix decreases with increasing temperature. As temperature increases, the thermal diffusivity decreases more rapidly, indicating thermally activated viscous flow of the glass allows the cavity formation.

The thermal diffusivity and thermal conductivity of a uniaxial carbon fiber reinforced lithia-aluminosilicate glass-ceramic are compared to those of the glass-ceramic. The thermal diffusivity and thermal conductivity parallel to the fibers are about twenty times higher than those of the glass-ceramic. The thermal diffusivity and thermal conductivity of the composite perpendicular to the fibers are higher than those of the glass ceramic at 25°C. At higher temperatures, the thermal diffusivity exhibits a permanent decrease after the first thermal cycle, and a hysteresis on subsequent thermal cycles. The permanent decrease is caused by the formation of large cracks through the matrix, which tend to follow the fiber-matrix interface where possible. The hysteresis

is probably caused by widening of the cracks as the temperature increases to about 600°C, then closing of the cracks as the temperature increases to 1000°C. The formation of the cracks could be due to residual stresses after processing due to the thermal expansion mismatch of the fibers and the glass-ceramic. Residual stresses could be caused by the approximately 6% decrease in volume of the matrix as it transformed from the glass to the glass-ceramic. Residual stresses could be caused by nonuniformity in the temperature of the billet as it cooled from the processing temperature to ambient temperature.

The modification of existing theories of the effective thermal conductivity of composites was done to include the effect of an interfacial resistance. The result also includes the size of the dispersions in the effective thermal conductivity. The consideration of spherical, cylindrical and parallel flat plate geometries are fundamental, and allow for further work on different composite geometries.

VIII. LITERATURE CITED

1. L. F. Johnson, D. P. H. Hasselman and K. Chyung, J. Am. Ceram. Soc., 70 (6) (1987) C135-C138.

2. L. F. Johnson, D. P. H. Hasselman, E. Minford, J. Mater. Sci. (in press).

3. D. P. H. Hasselman, L. F. Johnson, R. Syed, M. P. Taylor and K. Chyung, J. Mater. Sci. (in press).

4. D. P. H. Hasselman and L. F. Johnson, J. Comp. Mater. (in press).

5. W. J. Parker, R. J. Jenkins, C. P. Butler and G. L. Abbott, J. Appl. Phys., 32 (1961) 1679-1684.

6. H. W. Deem and W. D. Wood, Rev. Sci. Instr., 33 (1962) 1107-1109.

7. R. D. Cowan, J. Appl. Phys., 34 (1963) 926-927.

8. J. A. Cape and G. W. Lehman, J. Appl. Phys., 34 (1963) 1909-1913.

9. L. M. Clark III and R. E. Taylor, J. Appl. Phys., 46 (1975) 714-719.

10. R. C. Heckman, J. Appl. Phys., 44 (1973) 1455-1460.

11. J. A. Koski, "Improved Data Reduction Methods for Laser Pulse Diffusivity Determination with the use of Microcomputers," Thermal Conductivity 18 (Plenum Press, New York) (in press).

12. K. B. Larson and K. Koyama, J. Appl. Phys., 38 (1967) 465-474.

13. K. P. Gadkaree and K. Chyung, Am. Ceram. Soc. Bull., 65 (1986) 370-376.

14. A. E. Powers, "Conductivity in Aggregates," Knolls Atomic Power Laboratory Report KAPL-2145, March 6, 1961.

15. M. Srinivasan, L. D. Bentsen and D. P. H. Hasselman, "Thermal Diffusivity of Silicon Carbide-Silicon Carbide Composites," Thermal Conductivity 17 (Plenum Press, New York) pp 677-687. (1983).

16. K. M. Prewo, J. Mater. Sci., 17 (1982) 3549-3563.

17. M. S. Deshpande, R. H. Bogaard and R. E. Taylor, Int. J. Thermophysics 2 (1981) 357-370.

18. R. E. Taylor, High Temp. - High Pressures 15 (1983) 299-309.

19. J. Heremans, C. P. Beetz, I. Rahim, M. S. Dresselhaus, Thermal Conductivity 19 (Plenum Press, New York) (in press).

20. W. D. Kingery, J. Am. Ceram. Soc., 42 (1959) 617-627.

21. W. D. Kingery, H. K. Bowen and D. R. Uhlmann, Introduction to Ceramics, 2nd Ed. (Wiley press, New York) 1976. pp 630-634.

22. S. Nasu, T. Takahashi and T. Kikuchi, J. Nucl. Mater., 43 (1972) 72-74.

23. T. Tanaka and H. Susuki, Carbon, 10 (1972) 253-257.

24. M. R. Null, W. W. Lozier and A. W. Moore, Carbon, 11 (1973) 81-87.

25. Lord Raleigh, Phil. Mag., 34 (1892) 481-507.

26. E. B. Shand, Glass Engineering Handbook, 3rd Ed. (McGraw-Hill, New York) (1984).

27. J. J. Brennan, L. D. Bentsen and D. P. H. Hasselman, J. Mater. Sci., 17 (1982) 2337-2342.

28. D. P. H. Hasselman, J. Comp. Mater., 12 (1978) 403-407.

29. Y. Tree, A. Venkateswaran and D. P. H. Hasselman, J. Mater. Sci., 18 (1983) 2135-2148.

30. Y. S. Touloukian and E. H. Buyco, eds., Thermophysical Properties of Matter Vol. 5, Specific Heat of Nonmetallic Solids (IFI/ Plenum Publishing Co., New York) 1970.

31. S. G. Bapat, Carbon, 11 (1973) 511-514.

32. C. N. Hooker, A. R. Ubbelohde and D. A. Young, Proc. Royal Soc. London, A284 (1965) 17.

33. A. de Comberieu, J. Physics, 28 (1967) 951.

34. R. Taylor, Phil. Mag., 13 (1966) 157.

35. M. G. Holland, C. A. Klein and W. D. Straub, J. Phys. Chem. Solids, 27 (1966) 903.

36. B. Nysten, L. Piraux and J. P. Issi, Thermal Conductivity 20 (Plenum Press, New York) (in press).

37. J. C. Maxwell, A Treatise on Electricity and Magnetism Vol. 1, 3rd Ed. (Dover Publications, New York) 1954.

38. H. Fricke, Phys. Rev., 24 (1924) 575-587.

39. D. A. G. Bruggeman, Ann. Phys., 24 (1935) 636-679.

40. E. H. Kerner, Proc. Phys. Soc. (london), B69 (1956) 802.

41. R. E. De La Rue and C. W. Tobias, J. Electrochem. Soc., 106 (1959) 827.

42. Z. Hashin, J. Comp. Mater., 2 (1968) 284.

43. S. C. Cheng and R. I. Vachon, Int. J. Heat Mass Trans., 12 (1969) 249.

44. B. Budiansky, J. Comp. Mater., 4 (1970) 286.

45. A. Nir and A. Acrivos, J. Fluid Mech., 78 (1976) 33.

46. R. A. Crane and R. I. Vachon, Int. J. Heat Mass Trans., 20 (1977) 11.

47. S. Nomura and T. W. Chou, J. Comp. Mater., 14 (1980) 120.

48. H. Hata and M. Taya, J. Appl. Phys., 59 (1986) 1851.

49. B. R. Powell, Jr., G. E. Youngblood, D. P. H. Hasselman and L. D. Bentsen, J. Am. Ceram. Soc. 63 (1980) 581.

50. J. R. Willis, J. Mech. Phys. Solids, 25 (1977) 185.

51. H. J. Lee and R. E. Taylor, Thermal Conductivity 14 (Plenum Press, New York) 1976. pp 423-434.

52. A. Malliaris and D. T. Turner, J. Appl. Phys., 42 (1971) 614.

53. S. M. Aharoni, J. Appl. Phys., 43 (1972) 2463.

54. R. E. Meredith and C. W. Tobias, J. Appl. Phys., 31 (1960) 1270.

The vita has been removed from the scanned document